UNIVERSIDAD DE GRANADA

DEPARTAMENTO DE FÍSICA ATÓMICA,
MOLECULAR Y NUCLEAR

PROGRAMA DE DOCTORADO
BIOINGENIERÍA Y FÍSICA MÉDICA

Tesis de Doctorado

Obtención de los factores de corrección de cámaras de ionización de uso en dosimetría física

Fabián Erazo Caluquí

Noviembre 2015

Editor: Universidad de Granada. Tesis Doctorales
Autor: Fabián Gonzalo Erazo Caluquí
ISBN: 978-84-9125-657-1
URI: http://hdl.handle.net/10481/43404

El doctorando, Fabián Erazo Caluquí, autor de la presente tesis doctoral, titulada "Obtención de los factores de corrección de cámaras de ionización de uso en dosimetría física", y Antonio M. Lallena Rojo, director de la misma

GARANTIZAMOS que

1. el trabajo ha sido realizado por el primero bajo la dirección del segundo, y
2. hasta donde nuestro conocimiento alcanza, en la realización del trabajo, se han respetado los derechos de otros autores a ser citados, cuando se han utilizado sus resultados o publicaciones.

Y para que así conste a los efectos oportunos, firmamos el presente documento en Granada, a 30 de octubre de 2015

El director de la tesis	El doctorando
	
Fdo.: Antonio M. Lallena Rojo	Fdo.: Fabián Erazo Caluquí

A Patricia y Paula, mi familia, por su comprensión.

A Iván Andrés cuya partida no logro entender.

Agradecimientos

El presente trabajo de investigación ha sido desarrollado gracias al aporte de muchas personas sin las cuales no hubiese sido posible finalizarlo. De manera especial quiero agradecer a Antonio Lallena por su convicción inquebrantable como docente que ha hecho posible a través su dirección finalizar esta tesis doctoral. Gracias infinitas Antonio.

Un reconocimiento especial a Marta Anguiano por sus enseñanzas y su trabajo a través de los sistemas informáticos del departamento que han permitido los cálculos de esta investigación. También a los profesores del programa de doctorado que a lo largo de sus clases me han hecho comprender de qué se trata la investigación científica.

A José María Fernández Varea y Josep Sempau un reconocimiento especial por su bondad para discutir con una apertura magnífica los procesos de simulación, en sus despachos, en Barcelona.

Existen numerosas personas más que han colaborado de manera desinteresada en mi formación en la Universidad de Granada. Quisiera mencionar a todas y cada una de ellas y si omito a alguien me disculpo anticipadamente pero no ha sido mi intención evitar mencionarlas.

Al Organismo Internacional de Energía Atómica mediante los buenos oficios del Dr. Francisco Enríquez Guerra, coordinador general de esta institución en la ciudad de Cuenca, por su confianza y apoyo económico para los primeros años de formación. Al Instituto del Cáncer SOLCA Cuenca, de manera especial a su director el Dr. Raúl Alvarado Corral, quien con su visión me ha apoyado de manera absoluta en realizar este programa de doctorado sin pedir más que los conocimientos sean revertidos en su Institución.

El desarrollo del trabajo científico ha sido posible gracias a personas que han contribuido de manera altruista. A Brian Hooten de Standard Imaging por proveernos de los *blue prints* de las cámaras de ionización para que pudiéramos simularlas. A Llorenç Brualla que nos ha facilitado las geometrías de los aceleradores lineales para poder calcular los espacios de fases. Al profesor David Rogers del Ottawa Carleton Institute for Physics que ha compartido datos y recomendaciones para nuestro trabajo.

No quiero dejar de mencionar a mis compañeros de formación clínica en mi estancia en Madrid en el Hospital La Milagrosa: Cristina Mínguez, Alicia Sánchez, María Luisa Brosed, David Sevillano, Elena Sánchez, José Miguel Delgado, Raúl Matute, César Beltrán y Rosa Morera.

Finalmente reconocer en mis compañeros del programa de doctorado a seres extraordinarios y agradecer su amistad que perdura: Uriel, Paola, Segundo.

A la Granada de Francisco de Icaza: “Dale limosna, mujer, que no hay en la vida nada como la pena de ser ciego en Granada”. A Álvaro, Aurora, Joaquina y Jóse que hicieron de mi estancia algo maravilloso.

Índice general

Introducción

Hoy día se acepta que, en media, un 50 % del total de pacientes diagnósticados de cáncer deberían recibir radioterapia como parte de su tratamiento, aunque el porcentaje concreto puede variar mucho en función de la patología [1]. En radioterapia se pretende administrar una dosis de radiación a los tejidos tumorales evitando al máximo la irradiación de los tejidos normales circundantes [2]. Este proceso involucra diferentes etapas y procedimientos que tienen que ser realizados de acuerdo con los criterios establecidos en alguno de los protocolos reconocidos internacionalmente. A este respecto hay que señalar que son dos los más usados en los departamentos de física médica: el TRS-398 de la Agencia Internacional de Energía Atómica (IAEA) [3] y el TG-51 de la Asociación Americana de Físicos en Medicina [4].

En la práctica clínica actual se asume que la incertidumbre de los tratamientos de radioterapia debe ser del 5 % como máximo, un requerimiento que viene impuesto desde la práctica clínica y está basado, por tanto, en la evidencia de la relación entre la dosis prescrita y las probabilidades de control tumoral y de complicación del tejido normal. Así, los datos disponibles al respecto indican que un cambio de un 5 % en la dosis prescrita a los pacientes de radioterapia puede producir cambios del orden del 10 al 20 % en la probabilidad de control tumoral y del 20 al 30 % en la probabilidad de complicación del tejido normal [5]. Por ello, todos las etapas y procedimientos del proceso de radioterapia a que antes hemos hecho referencia deben ser evaluados de manera sistemática para que la incertidumbre total no exceda el máximo aceptado.

La dosimetría física es uno de esos procedimientos. Su objetivo fundamental es la caracterización de los haces de radiación que se emplean en radioterapia, es decir, el establecimiento de una colección de parámetros físicos que caracterizan las unidades de tratamiento, y que posteriormente sirven como referencia para futuras comprobaciones de la estabilidad y la repetibilidad de dichas unidades.

La dosimetría física de referencia, así como los posteriores controles dosimétricos, deben por tanto llevarse a cabo de acuerdo con protocolos de calibración de manera que sea posible no sólo alcanzar el objetivo global de precisión, sino también permitir una comparación de los resultados dosimétricos obtenidos en diferentes instituciones. En principio el procedimiento podría llevarse a cabo con distintos tipos de detectores de radiación, como dosímetros termoluminiscentes, dosímetros MOSFET, película radiocrómica, cámaras de ionización, etc. Sin embargo, son estas últimas las más ampliamente utilizadas en física médica, dadas su versatilidad, estabilidad y repetibilidad en las medidas, su fácil lectura y su relativo bajo coste, debido a su diseño simple, que permite el acceso a ellas de prácticamente cualquier usuario. En los dos protocolos citados la dosimetría física está basada

en parámetros de dosis absorbida en agua y se recomienda utilizar cámaras de ionización para su determinación.

Sin embargo existe un problema importante: este tipo de dosímetros deben estar calibrados para el haz con el que el usuario realizará las medidas y eso no es posible en la mayoría de los casos, ya que los laboratorios (primarios o secundarios) encargados de la certificación de calibración no disponen de todas y cada una de las calidades de haz utilizadas en las distintas unidades de radioterapia. Por ello, las cámaras de ionización se calibran por regla general en un haz de referencia, usualmente de ^{60}Co, y es necesario por tanto un factor de corrección que permita establecer la correspondiente calibración para la calidad de haz de interés para el usuario. Ese factor se denomina *factor de corrección de calidad de haz* y se denota como $k_{\mathrm{Q,Q_0}}$, con $\mathrm{Q_0}$ la calidad a la que la cámara ha sido calibrada en el laboratorio de calibración y Q la calidad del haz utilizado por el usuario. El factor de corrrección $k_{\mathrm{Q,Q_0}}$ está descrito con detalle en los protocolos [3,4].

Existen dos posibilidades para determinar los factores $k_{\mathrm{Q,Q_0}}$: de forma experimental, usando métodos dosimétricos absolutos, como calorímetros o dosímetros químicos, o con métodos numéricos, esencialmente usando técnicas Monte Carlo. En general, los métodos experimentales se basan en la independencia de la respuesta de los dispositivos de medida utilizados con la energía de la radiación considerada, por lo que serían útiles para cualquier usuario clínico. Sin embargo, no suelen estar disponibles en los departamentos de física médica debido a los requerimientos experimentales que conllevan y que solo pueden encontrarse en laboratorios de calibración. Eso hace que sean los valores obtenidos mediante simulación Monte Carlo los que usualmente se consideran en la práctica clínica. En cualquier caso los valores de los factores de corrección reportados en la bibliografía mediante métodos experimentales están en buen acuerdo con los obtenidos mediante Monte Carlo [4].

En esta tesis doctoral hemos abordado el cálculo de coeficientes de corrección para distintas cámaras y para haces de electrones y fotones de uso clínico con técnicas Monte Carlo, usando para ello el código de simulación PENELOPE [6] y considerando lo establecido en el protocolo TRS-398 [3].

En el capítulo 1 se introducen los factores de correción $k_{\mathrm{Q,Q_0}}$ de acuerdo a lo establecido en el protocolo dosimétrico de la IAEA. Además se hace una breve revisión de los métodos experimentales utilizados para su determinación. Finalmente se describen algunas de las características relevantes del código PENELOPE y algunos detalles de los cálculos que se han llevado a cabo.

En el capítulo 2 se estudian varias cámaras de tipo dedal (cilíndricas). Entre ellas se analiza la NE2571 (QADOS, Sandhurst, Reino Unido), considerada como cámara de referencia en el protocolo TRS-398. Los resultados obtenidos se comparan con los valores de otros autores para comprobar el método de cálculo usado y determinar las posibles diferencias debidas al código con el que se llevan a cabo las simulaciones. Se consideran tanto espectros de radiación de diferentes aceleradores lineales como haces monoenergéticos con el fin de estudiar la compatibilidad de los correspondientes resultados. Además se calculan los factores de corrección $k_{\mathrm{Q,Q_0}}$ para las cámaras A19 y A12S, de Standard Imaging (Middleton, E.E.U.U.), con los dos tipos de fuentes de radiación.

En el capítulo 3 se estudian cámaras plano-paralelas, calculando en primer lugar los factores de corrección de una de las cámaras de referencia para la dosimetría de electrones en radioterapia: la NACP-02 (IBA-Scanditronix, Louvain-la-Neuve, Bélgica). Los resultados obtenidos son comparados con los valores publicados en la bibliografía y con los disponibles en el protocolo TRS-398. A continuación se hace un estudio de varias cámaras plano-paralelas de Standard Imaging que, hasta donde nuestro conocimiento alcanza, no estaban aún caracterizadas. Estas cámaras son las siguientes: A10, A11, A11TW, P11, P11TW, T11 y T11TW. El estudio se lleva a cabo utilizando los espacios de fase generados para un acelerador Clinac 2100 C/D de Varian y también haces monoenergéticos sintonizados para reproducir los mismos valores de R_{50} que los de los haces realistas.

En el capítulo 4 se lleva a cabo la caracterización de las nuevas cámaras de ionización NE2571A y NE2581A, ambas de QADOS, que son de tipo dedal. Estás cámaras fueron presentadas por el fabricante como reemplazo de las cámaras de referencia NE2571 y NE2581. Los resultados obtenidos para las nuevas cámaras se comparan con los correspondientes a las anteriores estableciendo las diferencias existentes.

Finalmente en el capítulo 5 se presentan las conclusiones de este trabajo de investigación y se enuncian las perspectivas del mismo.

Se estima que la dosimetría física de referencia tiene asociada una incertidumbre de entre el 1 y el 2 %, siempre y cuando sea llevada a cabo con el mayor rigor posible [7]. Esto pone de manifiesto la importancia que tendría cualquier mejora que pudiera alcanzarse en la precisión del propio proceso, mejora que es el objetivo último del tipo de cálculos realizados en esta tesis.

---

[1] Delaney G, Jacob S, Featherstone C, Barton M. The role of radiotherapy in cancer treatment: estimating optimal utilization from a review of evidence-based clinical guidelines. Cancer. 2005; 104:1129-37.

[2] Almond PR. A historical perspective: A brief history of dosimetry, calibration protocols and the need for accuracy in clinical dosimetry measurements in radiotherapy. 2009 AAPM Summer School. Colorado Springs: AAPM; 2009.

[3] International Atomic Energy Agency. Absorbed dose determination in external beam radiotherapy, IAEA Technical Reports Series 398. Vienna: IAEA; 2000.

[4] Almond PR, Biggs PJ, Caursey BM, Hanson WF, Saiful HM, Nat R, Rogers DWO. AAPM's TG-51 protocol for clinical reference dosimetry of high-energy photon and electron beams. Med Phys 1999; 26: 1847-70.

[5] Bentzen SM. Dose-response relationships in radiotherapy. In "Basic clinical radiobiology", 3rd edition. Ed. G Gordon Steel. Londres: Arnold, 2002; p 94-104

[6] Salvat F, Fernández-Varea JM, Sempau J. PENELOPE 2011: A code system for Monte Carlo simulation of electron and photon transport. Issy-les-Moulineaux: OECD Nuclear Energy Agency; 2011.

[7] International Commission on Radiation Units and Measurements. Determination of absorbed dose in a patient irradiated by beams of X or gamma rays in radiotherapy procedures, ICRU Report 24. Bethesda: Oxford University Press; 1976.

Capítulo 1

Dosimetría en radioterapia

En este capítulo se introduce el factor de calidad de haz de acuerdo con lo establecido en el protocolo TRS-398, del Organismo Internacional de la Energía Atómica [1], que es el que hemos utilizado en este trabajo. Después de una breve revisión de los métodos experimentales utilizados para determinar $k_{\mathrm{Q,Q_0}}$, se describen algunas de las características del código Monte Carlo PENELOPE que es el que hemos utilizado en nuestros cálculos, así como algunos detalles relativos a los mismos.

1.1. El protocolo TRS-398

El protocolo TRS-398 del IAEA [1] se basa esencialmente en la teoría de la cavidad de Spencer–Attix para dar solución al problema de la dosimetría física cuando se utilizan cámaras de ionización tanto cilíndricas como plano-paralelas. La teoría se desarrolló originalmente para medios irradiados con fotones, asumiendo que se verificaba el equilibrio de partículas cargadas en el propio medio en la posición en la que la cavidad estaba situada, pero también se puede aplicar a medios irradiados con neutrones o con partículas cargadas, como electrones y protones.

En concreto, la teoría de Spencer–Attix permite determinar la energía que se deposita en una cavidad de Bragg–Gray, que se considera como detector. Una cavidad de Bragg–Gray es una cavidad muy pequeña que cumple que (i) la energía que se deposita en la misma, debida a los electrones generados dentro de ella por fotones que la alcanzan, es despreciable frente a la debida a aquellos electrones producidos por fotones en el medio que rodea, y (ii) la fluencia de los electrones que atraviesan la cavidad es la misma que la que existiría en el medio, en el mismo punto de interés, si la cavidad no estuviera presente.

El protocolo TRS-398 [1] aplica la teoría de Spencer–Attix considerando una cavidad de aire en el seno de agua por lo que, en el caso de una cavidad de Bragg–Gray ideal, es posible relacionar la dosis absorbida en agua, $D_{\mathrm{w,Q}}$, para una calidad de haz dada Q, con la dosis absorbida en la cavidad, $D_{\mathrm{air,Q}}$, mediante la razón de poderes de frenado entre agua y aire, $(S_{\mathrm{w,air}})_{\mathrm{Q}}$:

$$D_{\mathrm{w,Q}} \;=\; D_{\mathrm{air,Q}} \cdot (S_{\mathrm{w,air}})_{\mathrm{Q}} \,. \tag{1.1}$$

Como las cámaras de ionización reales muestran desviaciones respecto del comportamiento de una cavidad de Bragg–Gray ideal, la ecuación anterior se modifica introduciendo un factor de perturbación, $p_{\mathrm{c,Q}}$, que da cuenta de esas desviaciones:

$$D_{\mathrm{w,Q}} \;=\; D_{\mathrm{c,Q}} \cdot p_{\mathrm{c,Q}} \cdot (S_{\mathrm{w,air}})_{\mathrm{Q}} \,, \tag{1.2}$$

donde ahora se ha introducido $D_{c,Q}$, que es la dosis absorbida en la cámara de ionización. El factor de perturbación $p_{c,Q}$ se puede factorizar en cuatro términos: p_{wall}, que tiene en cuanta el hecho de que las paredes de la cámara de ionización no son equivalentes al agua; p_{cav}, que corrige por las diferencias en la fluencia electrónica en la cavidad de aire de la cámara respecto de la que se tendría en agua en ausencia de la propia cámara; p_{dis}, que considera el cambio en el punto efectivo de medida debido a que un cierto volumen de agua es sustituido por el aire de la cavidad, y p_{cel}, que corrige la respuesta de la cámara por el efecto debido al electrodo central de la misma. De acuerdo con el reporte 64 de ICRU [2] se asume que estos factores son independientes y son considerados como perturbaciones de primer orden.

Además de la condición antes indicada acerca de la necesidad de que la fluencia electrónica en el punto de medida sea la misma tanto si el detector está presente como si no es así, la aplicación de la ecuación anterior requiere que $p_{c,Q}$ y $(S_{w,air})_Q$ no estén correlacionados. Por ello se ha propuesto una expresión alternativa en la que la dosis absorbida en agua, $D_{w,Q}$, se relaciona directamente con la dosis absorbida en el detector, $D_{c,Q}$ [3,4]:

$$D_{w,Q} = D_{c,Q} \cdot f_{c,Q} \,. \tag{1.3}$$

La ventaja de este procedimiento es evidente: el factor global, $f_{c,Q}$, se puede calcular usando una descripción realista de la geometría del detector y, además, tiene en cuenta, de manera directa y en su totalidad, el efecto completo debido a la presencia del detector en el seno del medio.

De acuerdo con el protocolo TRS-398 los usuarios de cámaras de ionización pueden determinar directamente la dosis absorbida en agua cuando la irradiación se realiza con un haz de referencia, generalmente el obtenido de una fuente de ^{60}Co, mediante la siguiente ecuación:

$$D_{w,Q_0} = M_{Q_0} \cdot N_{D,w,Q_0} \,, \tag{1.4}$$

donde M_{Q_0} es la lectura que arroja el electrómetro al que está conectada la cámara de ionización, corregida por los efectos de temperatura, presión, calibración del electrómetro, polaridad y recombinación iónica, y N_{D,w,Q_0} es el factor de calibración en términos de dosis absorbida en agua para la calidad de referencia Q_0. Los laboratorios de calibración dosimétrica, ya sean primarios o secundarios, calibran las cámaras de ionización y proporcionan el valor de N_{D,w,Q_0} en cGy/nC. Obviamente, lo ideal sería que el laboratorio de calibración pudiera realizar ésta utilizando la misma calidad de haz Q que posteriormente utilizará el usuario, estableciendo el factor de calibración para esa calidad $N_{D,w,Q}$ para el que se tendría:

$$D_{w,Q} = M_Q \cdot N_{D,w,Q} \,, \tag{1.5}$$

Como los laboratorios de calibración no disponen de todas las calidades utilizadas por los usuarios, esta última ecuación se modifica de manera que se tiene en cuenta la calidad Q_0 de referencia:

$$D_{w,Q} = M_Q \cdot N_{D,w,Q_0} \cdot k_{Q,Q_0} \,, \tag{1.6}$$

donde k_{Q,Q_0} es el factor de corrección de calidad de haz antes mencionado y depende de la cámara de ionización concreta que se considere.

Según la teoría de la cavidad de Spencer–Attix, este factor de corrección viene dado por:

$$k_{\mathrm{Q},\mathrm{Q}_0} = \frac{(S_{\mathrm{w,air}})_{\mathrm{Q}}}{(S_{\mathrm{w,air}})_{\mathrm{Q}_0}} \cdot \frac{p_{\mathrm{c,Q}}}{p_{\mathrm{c,Q}_0}}\,, \tag{1.7}$$

o bien, de acuerdo con los trabajos de Sempau *et al.* [3] y de Capote *et al.* [4] antes mencionados,

$$k_{\mathrm{Q},\mathrm{Q}_0} = \frac{f_{\mathrm{c,Q}}}{f_{\mathrm{c,Q}_0}}\,. \tag{1.8}$$

Esta es la expresión que utilizamos en este trabajo para calcular el factor de corrección $k_{\mathrm{Q},\mathrm{Q}_0}$.

1.2. Determinación experimental de $k_{\mathrm{Q},\mathrm{Q}_0}$

Si tenemos en cuenta las ecuaciones (1.4) y (1.6) podemos escribir:

$$k_{\mathrm{Q},\mathrm{Q}_0} = \frac{D_{\mathrm{w,Q}}}{D_{\mathrm{w,Q}_0}} \cdot \frac{M_{\mathrm{Q}_0}}{M_{\mathrm{Q}}}\,. \tag{1.9}$$

Una vez medidas las dosis absorbidas en agua experimentalmente, se utiliza esta expresión para determinar el factor $k_{\mathrm{Q},\mathrm{Q}_0}$ de una cámara de ionización dada.

Existen básicamente dos procedimientos con los que se puede medir la dosis en agua: la calorimetría en agua y los métodos químicos.

En la dosimetría basada en calorimetría en agua, la tasa de dosis absorbida es medida de forma directa en el agua. Como esa medida es, a la vez, absoluta, el calorímetro no debe ser calibrado con respecto a un estándar primario de radiación.

La utilización del calorímetro se basa en suponer que toda la energía absorbida por el medio irradiado se traduce en un incremento de su temperatura [5]. Bajo esta hipótesis fundamental es posible establecer una relación entre la tasa de dosis absorbida en agua, $\dot{D}_{\mathrm{w}}$, y la tasa de incremento de la temperatura del agua, $\Delta\dot{T}$:

$$\dot{D}_{\mathrm{w}} = (c_{\mathrm{w}})_P \cdot \Delta\dot{T} \cdot \kappa\,, \tag{1.10}$$

donde $(c_{\mathrm{w}})_P$ es la capacidad calorífica específica del agua, a presión constante y κ es un factor de corrección que tiene en cuenta la transferencia de calor debida a efectos de conducción y convección en el agua, los defectos de calor debidos a posibles reacciones químicas en el agua producidas por la presencia de impurezas y las perturbaciones en la distribución de dosis debidas a los materiales diferentes al agua presentes en el arreglo experimental [5]. Este método es generalmente usado en los laboratorios primarios de calibración para verificar los patrones de dosis absorbida en agua y no es un método al alcance de los servicios de radiofísica hospitalaria.

La dosimetría química consiste en utilizar cambios químicos producidos por la radiación en los materiales, de forma que se pueda cuantificar de manera directa o indirecta la

energía depositada en el proceso de irradiación. Uno de los procedimientos más utilizados es la dosimetría de Fricke, que se basa en la irradiación de un vial, situado en un maniquí de agua en la posición de medida, que contiene una solución de sulfato ferroso amónico y cloruro sódico en ácido sulfúrico y agua bidestilada. Tras la irradiación, los iones Fe^{2+} se transforman en iones Fe^{3+} y el cambio en la concentración de estos últimos permite determinar la dosis absorbida [6].

Otros dosímetros químicos muy utilizados son los de alanina que es un aminoácido que, cuando se irradia, pierde el grupo NH_2^-, dando lugar a radicales estables libres cuya concentración es proporcional a la dosis absorbida y puede medirse mediante espectroscopía por resonancia paramagnética de electrones. La muestra que se irradia se construye con *pellets*, de 5 mm de diámetro y ~ 2.5 mm de espesor, de una mezcla de alanina con un 10 % de parafina, que se introducen en una varilla de PMMA u otro material similar [7].

Si se dispone de una cámara calibrada, es decir, de la que se conoce el factor de calibración $N_{D,\mathrm{w},\mathrm{Q}_0}$ para la calidad de referencia Q_0, es posible determinar el factor de corrección para otra cámara de ionización comparando directamente las ionizaciones medidas con ambas cámaras. De acuerdo con la ecuación (1.9) podemos escribir que el correspondiente factor de corrección para la cámara calibrada viene dado por:

$$k^{\mathrm{cal}}_{\mathrm{Q},\mathrm{Q}_0} = \frac{D_{\mathrm{w},\mathrm{Q}}}{D_{\mathrm{w},\mathrm{Q}_0}} \cdot \frac{M^{\mathrm{cal}}_{\mathrm{Q}_0}}{M^{\mathrm{cal}}_{\mathrm{Q}}} \,. \tag{1.11}$$

Y teniendo en cuenta las ecuaciones (1.9) y (1.11), podemos obtener el factor de corrección de la cámara problema como

$$k_{\mathrm{Q},\mathrm{Q}_0} = \frac{M_{\mathrm{Q}_0}}{M_{\mathrm{Q}}} \cdot \frac{M^{\mathrm{cal}}_{\mathrm{Q}}}{M^{\mathrm{cal}}_{\mathrm{Q}_0}} \cdot k^{\mathrm{cal}}_{\mathrm{Q},\mathrm{Q}_0} \,. \tag{1.12}$$

Por lo tanto lo único que en teoría quedaría por hacer es medir, bajo las mismas condiciones de irradiación, las ionizaciones producidas en ambas cámaras para las dos calidades de haz, Q y Q_0 [8].

1.3. Cálculo Monte Carlo de $k_{\mathrm{Q},\mathrm{Q}_0}$

En general, la determinación experimental del factor de corrección $k_{\mathrm{Q},\mathrm{Q}_0}$ es complicada y por ello se suelen utilizar valores tabulados del mismo obtenidos a partir de cálculos Mone Carlo. En este trabajo hemos abordado el problema desde este punto de vista y hemos llevado a cabo el cálculo de los factores de corrección de calidad de haz, para distintas cámaras de ionización y para haces de electrones y fotones de varias energías, usando el código PENELOPE [9].

1.3.1. El código PENELOPE

En términos generales, la simulación Monte Carlo del transporte de radiación en medios materiales consiste en el seguimiento de las historias de las partículas que forman el haz de radiación a su paso por el material en cuestión. La base de ese seguimiento (simulación) está en considerar los distintos mecanismos de interacción puestos en juego, que están descritos a través de las correspondientes secciones eficaces de interacción. La naturaleza intrínsecamente aleatoria de esos procesos de interacción permite su análisis mediante técnicas Monte Carlo de manera natural.

En cada interacción la partícula incidente sufre (o puede sufrir) un cambio de dirección o una pérdida de energía que puede ser transferida, total o parcialmente, al medio, pudiendo dar lugar a la generación de nuevas partículas (partículas secundarias) cuyas respectivas historias deberán también ser consideradas. Todos estos detalles específicos están descritos a través de las secciones eficaces antes mencionadas.

Existen varios códigos de simulación Monte Carlo del transporte de radiación en medios materiales disponibles. Los códigos EGS4, desarrollado por Nelson *et al.* en 1985 [10], ETRAN, publicado por Berger y Seltzer en 1988 [11], ITS3, de Halbleib *et al.*, aparecido en 1992 [12], PENELOPE, cuya primera versión data de 1996 [9], y EGSnrc, de Kawrakow *et al.*, publicado en 2001 [13], permiten simular el transporte acoplado de electrones, fotones y positrones. Otros códigos con los que es posible simular, además, otras partículas, como neutrones, protones, partículas α o iones pesados, son MCNP (con sus distintas versiones) [14], Geant4 [15] y FLUKA [16].

PENELOPE, acrónimo de "**PEN**etration and **E**nergy **LO**ss of **P**ositrons and **E**lectrons in matter" [9], es el código utilizado en este trabajo de investigación. Originalmente, sólo incluía el transporte de electrones y positrones; el de fotones se añadió posteriormente. PENELOPE permite realizar el transporte de las partículas mencionadas con energías comprendidas entre unos 50 eV y 1 GeV.

En el caso de fotones, los mecanismos de interacción que PENELOPE tiene en cuenta son el efecto fotoeléctrico, la dispersión (coherente) Rayleigh, la dispersión (incoherente) Compton y la producción de pares electrón–positrón. Por su parte, electrones y positrones pueden sufrir dispersiones elásticas, dispersiones inelásticas, emisión Bremsstrahlung. En el caso de los positrones también se considera la aniquilación. En PENELOPE estos procesos de interacción se describen mediante las correspondientes secciones eficaces diferenciales que están obtenidas a partir de bases de datos experimentales o calculadas o de modelos teóricos contrastados [9].

La simulación de las historias de fotones se realiza en PENELOPE, igual que en los restantes códigos Monte Carlo antes mencionados, de forma detallada, es decir, simulando de forma cronológica todos y cada uno de los eventos de interacción que cada fotón sufre con el material en el que se está moviendo. En este caso, la simulación detallada es viable ya que la historia de un fotón es corta y se termina generalmente después de unas cuantas interacciones.

Sin embargo la simulación de las historias de electrones o positrones no pueden llevarse a cabo en forma detallada de manera sencilla, ya que la pérdida de energía que estas partículas sufren en cada interacción es relativamente muy pequeña, lo que implica que es necesario un número considerable de interacciones hasta que los electrones o los positrones alcanzan energías por debajo de las energías de absorción que se hayan establecido previamente.

Para superar este problema los códigos Monte Carlo recurren a las teorías de dispersión múltiple en las cuales el efecto global de un cierto número de eventos de dispersión se describe de manera condensada. Estas teorías de dispersión múltiple son, evidentemente, aproximaciones de la realidad y podrían conducir a errores sistemáticos en aquellos casos en los que el número de interacciones de las partículas simuladas es pequeño como sucede en el caso del trasnporte en láminas materiales delgadas como las que, por ejemplo, se encuentran en la simulación de la respuesta de cámaras de ionización [9].

PENELOPE simula las trayectorias de los electrones y positrones separando las interacciones que sufren en dos grupos: duras y blandas. Las colisiones duras son aquéllas en las que los cambios de dirección de la trayectoria de la partícula o las pérdidas de energía sufridas por ella son mayores que ciertos valores umbral definidos por el usuario; las interacciones blandas son las que no cumplen esas condiciones. Mientras que las interacciones duras son simuladas en forma detallada, el efecto combinado de todas las interacciones blandas que ocurren entre dos interacciones duras se simula mediante un evento singular artificial caracterizado por el modelo de dispersión múltiple correspondiente.

Para llevar a cabo la simulación, PENELOPE requiere leer la información física de cada material que interviene en la geometría en la que se lleva a cabo. La información sobre los materiales se genera mediante el programa auxiliar `material`, que requiere información específica acerca del material: composición estequiométrica o fracción en peso de cada elemento constituyente del material, densidad másica, energía media de excitación, etc. En el caso de los elementos compuestos se utiliza la aproximación de aditividad para definir la sección eficaz de los materiales. PENELOPE tiene una base de datos de 280 elementos precalculados [9].

Evidentemente PENELOPE requiere también la geometría sobre la cual se realiza el transporte de radiación. Para construirla se utilizan superficies cuádricas que delimitan regiones del espacio que son "llenadas" con los materiales concretos. La manipulación de las geometrías se lleva a cabo mediante el paquete de subrutinas `pengeom`, que es parte de la distribución del programa.

En cada instante de la simulación de una historia de una partícula se requiere la determinación de la longitud de camino hasta la siguiente interacción, la determinación del proceso de interacción que la partícula sufrirá al final del salto y su estado tras sufrir esa interacción (posición, dirección de movimiento y energía). En cada salto entre interacciones, se deben realizar las operaciones geométricas necesarias, que involucran tareas como producir los desplazamientos espaciales y controlar el cruce de interfases entre materiales diferentes.

En esta última situación, `pengeom` trabaja de forma sencilla: cuando una partícula alcanza una interfase su trayectoria se detiene justo después de entrar en el nuevo material

y es de nuevo lanzada desde ese mismo punto, ya en el nuevo material. Este método logra optimizar la parte geométrica sin perjudicar el proceso físico del transporte de radiación en los diferentes medios materiales. Además se puede compatibilizar con la aproximación utilizada en PENELOPE para describir el conjunto de interacciones blandas descritas mediante teorías de dispersión múltiple.

Además de generar la geometría de simulación y los materiales que entran en juego en la misma, PENELOPE, que no es más que un conjunto de subrutinas escritas en FORTRAN, requiere un programa principal que controle todos los procedimientos necesarios y, consiguientemente, los correspondientes parámetros de simulación. La distribución de PENELOPE incluye dos programas principales de caracter genérico; `pencyl`, que permite realizar simulaciones en estructuras geométricas de simetría cilíndrica, y `penmain`, que es un programa de propósito general.

1.3.2. Características de las simulaciones realizadas

Además de los dos programas principales antes mencionados, hay disponible otro, también de propósito general, que se denomina `penEasy`, que fue desarrollado por Sempau *et al.* [17] y que es el que hemos utilizado en este trabajo para realizar las distintas simulaciones. El programa permite simular tanto partículas monoenergéticas como espectros, para los tres tipos de radiación permitidos (fotones, electrones o positrones). También es posible controlar la dirección de emisión desde la fuente, así como la apertura del "cono de emisión". Además se puede usar como fuente de partículas iniciales un espacio de fases previamente calculado (tanto en formato estándar del propio código como en el de la IAEA).

`penEasy` controla los parámetros de transporte de electrones/positrones para cada material que aparece en la geometría. Estos son: C_1, que está relacionado con la deflexión angular promedio, y C_2, que representa la máxima pérdida relativa de energía promedio, ambos calculados entre dos colisiones elásticas duras consecutivas; W_{cc} y W_{cr}, que corresponden a las energías umbral para las colisiones inelásticas duras y de emisión Bremsstrahlung dura, respectivamente, y $S_{\max}$, que define la longitud de paso máxima permitida entre interacciones.

Además es necesario fijar los valores de las energías de absorción para cada una de las partículas que pueden simularse, $E_{\mathrm{abs}}(e^-)$, $E_{\mathrm{abs}}(\gamma)$ y $E_{\mathrm{abs}}(e^+)$, que representan las energías mínimas para que la simulación de las correspondientes partículas continue. En cálculos de dosis absorbidas los valores de E_{abs} deben elegirse de tal manera que el alcance residual de las partículas con esa energía sea más pequeño que el volumen del *voxel* usado para registrar la distribución de dosis [9].

En cada uno de las simulaciones específicas que se analizan en los capítulos siguientes se indican los valores concretos de los parámetros de transporte utilizados.

Por otro lado, y como se ha indicado anteriormente, el cálculo del factor $k_{\mathrm{Q,Q_0}}$ se ha llevado a cabo usando el cociente dado por la ecuación (1.8):

$$k_{\mathrm{Q,Q_0}} = \frac{f_{\mathrm{c,Q}}}{f_{\mathrm{c,Q_0}}},$$

donde los respectivos factores globales se han determinado de acuerdo con la ecuación (1.3):

$$f_{\mathrm{c,Q}} \,=\, \frac{D_{\mathrm{w,Q}}}{D_{\mathrm{c,Q}}}\,, \quad f_{\mathrm{c,Q_0}} \,=\, \frac{D_{\mathrm{w,Q_0}}}{D_{\mathrm{c,Q_0}}}\,. \tag{1.13}$$

Con el fin de obtener los valores de dosis necesarios hemos hecho uso del *tally* de distribución de dosis cilíndrica y del de deposición de energía, ambos incluidos en `penEasy`. Con el primero, que permite determinar los perfiles de dosis en profundidad, hemos calculado $D_{\mathrm{w,Q}}$ y $D_{\mathrm{w,Q_0}}$; el segundo proporciona estimaciones de la energía depositada en cualquiera de los cuerpos materiales incluidos en la geometría y, en particular, nos ha permitido obtener los valores de $D_{\mathrm{c,Q}}$ y $D_{\mathrm{c,Q_0}}$.

El proceso de simulación Monte Carlo usando PENELOPE con los parámetros que se han utilizado en cada caso requiere un tiempo de CPU considerable. Para poder llevar a cabo las simulaciones en tiempos razonables, hemos hecho uso de la metodología propuesta en el trabajo de Badal y Sempau [18], según la cual cada simulación se divide en varias partes que se ejecutan en computadores diferentes, utilizándose posteriormente el programa `clonEasy` para reunir los resultados obtenidos en un valor único. En cada una de las simulaciones individuales, el generador de números aleatorios se inicializa con semillas diferentes, pertenecientes a la misma secuencia, garantizándose en todo caso que los cálculos no estén correlacionados. En nuestros cálculos hemos utilizado las diferentes unidades del cluster del departamento de Física Atómica, Molecular y Nuclear de la Universidad de Granada.

La estimación de incertidumbres se ha realizado de la siguiente forma. Supongamos que queremos estimar una cierta magnitud Q y que el cálculo se subdivide entre M procesadores. Cada uno de ellos proporciona como resultado de la simulación el valor

$$\bar{q}_i \,=\, \frac{1}{N_i}\sum_{k=1}^{N_i} q_k\,, \quad i = 1, 2, \ldots, M\,, \tag{1.14}$$

con una incertidumbre

$$\sigma_{q_i} \,=\, \sqrt{\frac{1}{N_i}\left[\frac{1}{N_i}\sum_{k=1}^{N_i} q_k^2 \,-\, \bar{q}_i^2\right]}\,. \tag{1.15}$$

En las ecuaciones anteriores N_i es el número de historias simuladas en el procesador i-ésimo, por lo que el número total de historias de la simulación completa es

$$N \,=\, \sum_{i=1}^{M} N_i \tag{1.16}$$

y la estimación Monte Carlo de la magnitud de interés viene dada por

$$\overline{Q} \,=\, \frac{1}{N}\sum_{k=1}^{N} q_k \,=\, \frac{1}{N}\sum_{i=1}^{M} N_i \cdot \bar{q}_i\,. \tag{1.17}$$

La incertidumbre asociada a esta estimación es:

$$\begin{aligned}\sigma_Q &= \sqrt{\frac{1}{N}\left[\frac{1}{N}\sum_{k=1}^{N} q_k^2 - \overline{Q}^2\right]} = \sqrt{\frac{1}{N}\left[\frac{1}{N}\sum_{i=1}^{M}\sum_{k=1}^{N_i} q_k^2 - \overline{Q}^2\right]} \\ &= \sqrt{\frac{1}{N}\left[\frac{1}{N}\sum_{i=1}^{M} N_i\left(\frac{1}{N_i}\sum_{k=1}^{N_i} q_k^2\right) - \overline{Q}^2\right]} \\ &= \sqrt{\frac{1}{N}\left[\frac{1}{N}\sum_{i=1}^{M} N_i\left(N_i\cdot\sigma_{q_i}^2 + \bar{q}_i^2\right) - \overline{Q}^2\right]}, \end{aligned} \tag{1.18}$$

donde hemos tenido en cuenta la ecuación (1.15).

[1] International Atomic Energy Agency. Absorbed dose determination in external beam radiotherapy, IAEA Technical Report Series 398. Vienna: IAEA; 2000.

[2] International Commission on Radiation Units & Measurements. Dosimetry of high-energy photon beams based on standards of absorbed dose to waterm (Report 64). J ICRU 2001; 1: 1. Bethesda: ICRU; 2001.

[3] Sempau J, Andreo P, Aldana J, Mazurier J, Salvat F. Electron beam quality correction factors for plane-parallel ionization chambers: Monte Carlo calculations using the PENELOPE system. Phys Med Biol 2004; 49: 4427-44.

[4] Capote R, Sánchez-Doblado F, Leal A, Lagares JI, Arráns R, Hartmann GH. An EGSnrc Monte Carlo study of the microionization chamber for reference dosimetry of narrow irregular IMRT beamlets. Med Phys 2004; 31: 2416-22.

[5] Sarfehnia A, Kawrakow I, Seuntjens J. Direct measurement of absorbed dose to water in HDR ^{192}Ir brachytherapy: water calorimetry, ionization chamber, Gafchromic film, and TG-43. Med Phys 2010; 37: 1924-32.

[6] Palm A, Mattsson O. Experimental determination of beam quality conversion factors k_{Q} in clinical photon beams using ferrous sulphate (Fricke) dosimetry. Med Phys 2002; 29: 2756-62.

[7] Schauer DA, Iwasaki A, Romanyukha AA, Swartz HM, Onori S. Electron paramagnetic resonance (EPR) in medical dosimetry. Radiat Meas 2007; 41: S117-23.

[8] Gonzalez DM, Hartmann GH, Sanchez Doblado D, Gómez F, Kapsch RP, Peña J, Capote R. The determination of beam quality correction factors: Monte Carlo simulations and measurements. Phys Med Biol 2009; 54: 4723-41.

[9] Salvat F, Fernández-Varea JM, Sempau J. PENELOPE 2011: A code system for Monte Carlo simulation of electron and photon transport. Issy-les-Moulineaux: OECD Nuclear Energy Agency; 2011.

[10] Nelson WR, Hirayama H, Rogers DWO. The EGS4 code system. Report SLAC-265. Stanford: Stanford Linear Accelerator Center; 1985.

[11] Berger MJ, Seltzer SM. Monte Carlo transport of electrons and photons. Jenkins TM, Nelson WR, Rindi A. eds. New York: Plenum; 1988.

[12] Halbleib JA, Kensek RP, Mehlhorn TA, Valdez GD, Seltzer SM, Berger MJ. ITS version 3.0: The integrated TIGER series of coupled electron/photon Monte Carlo transport codes. Albuquerque: Sandia National Laboratories; 1992.

[13] Kawrakow I, Rogers DWO. The EGSnrc code system: Monte Carlo simulation of electron and photon transport. Otawa: Report PIRS-701 National Research Council of Canada; 2001.

[14] X-5 Monte Carlo team. MCNP-A general Monte Carlo N-particle transport code, version 5. New Mexico: Los Alamos National Laboratory; 2003.

[15] Agostinelli S. *et al.* Geant4–a simulation toolkit. Nucl Instrum Meth Phys Res A 2003; 506: 250-303.

[16] Ferrari A, Sala PR, Fassó A, Ranft J. FLUKA: a multi-particle transport code (Program version 2005). CERN-2005-10, INFN/TC-05/11, SLAC-R-773. Geneva: CERN; 2005.

[17] Sempau J, Badal A, Brualla L. A PENELOPE based system for the automated Monte Carlo simulation of clinacs and voxelized geometries application to far from axis fields. Med Phys 2011; 38: 5887-95.

[18] Badal A, Sempau J. A package of linux scripts for the parallelizationof Monte Carlo simulations. Computer Physics Communications 2006; 175: 440-50.

Capítulo 2

Cámaras de dedal

Physica Medica: European Journal of Medical Physics 29 (2013) 163-170

Calculation of beam quality correction factors for various thimble ionization chambers using the Monte Carlo code PENELOPE

Fabián Erazo[1,2] and Antonio M Lallena[1]

[1] Departamento de Física Atómica, Molecular y Nuclear, Universidad de Granada, E-18071 Granada, Spain
[2] Instituto del Cáncer - SOLCA, Cuenca, Ecuador

The beam quality correction factor k_{Q,Q_0} and the perturbation factor p_Q, commonly considered in dosimetry with ionization chambers, were calculated for the NE2571 and the Standard Imaging A19 and A12S chambers, using the Monte Carlo simulation code PENELOPE. For the NE2571 chamber, the values of k_{Q,Q_0} obtained are in very good agreement with those found in previous works by Wulff et al. and Muir and Rogers with the code EGSnrc and also with the experimental results summarized in the NCS code of practice. For p_Q, a difference of $\sim 0.4\,\%$ have been found between our results and those obtained with EGSnrc for ^{60}Co and this difference increases slightly with TPR_{10}^{20} values. These factors have been calculated also for the A19 and A12S chambers of Standard Imaging. The values of k_{Q,Q_0} show reasonable agreement with those recently calculated by Muir and Rogers and the measurements of McEwen.

2.1. Introduction

TG51 [1] and TRS-398 [2], the common codes of practice for dosimetry in radiotherapy, recommend to determine the absorbed dose on the base of standards of dose to water. Using Spencer-Attix cavity theory, the dose in water, $D_{\mathrm{w,Q}}$, for a given beam quality Q, is related to the dose in an air cavity, $D_{\mathrm{air,Q}}$, by means of the stopping-power ratio between water and air, $(s_{\mathrm{w,air}})_{\mathrm{Q}}$:

$$D_{\mathrm{w,Q}} \;=\; D_{\mathrm{air,Q}} \cdot (s_{\mathrm{w,air}})_{\mathrm{Q}} \,. \tag{2.1}$$

However, the detector (usually an ionization chamber) differs from the ideal cavity considered in the theory and an overall perturbation factor, p_{Q}, must be included:

$$D_{\mathrm{w,Q}} \;=\; D_{\mathrm{c,Q}} \cdot p_{\mathrm{Q}} \cdot (s_{\mathrm{w,air}})_{\mathrm{Q}} \,, \tag{2.2}$$

where $D_{\mathrm{c,Q}}$ is the dose measured in the ionization chamber. This perturbation factor takes into account the fact that (i) the fluence in the medium (water) is different from that in the air cavity inside the ionization chamber; (ii) the air cavity of the ionization chamber produces a lower attenuation than the water it displaces and a shift of the effective measurement point; (iii) the material of the wall of the ionization chamber is different from that of the medium where measurements are performed, water in this case; (iv) a waterproofing sleeve can be eventually present; (v) the central electrode situated in the air cavity of the ionization chamber produces a perturbation, and (vi) ionization chambers usually have stems.

Also of interest is the so-called beam quality correction factor which takes into account that the quality Q of the final user is different from the quality Q_0 at which the ionization chamber is calibrated in the reference laboratory. This factor is given by [2]

$$k_{\mathrm{Q,Q_0}} \;=\; \frac{p_{\mathrm{Q}}}{p_{\mathrm{Q_0}}} \, \frac{(s_{\mathrm{w,air}})_{\mathrm{Q}}}{(s_{\mathrm{w,air}})_{\mathrm{Q_0}}} \;=\; \left(\frac{D_{\mathrm{w,Q}}}{D_{\mathrm{c,Q}}}\right) \cdot \left(\frac{D_{\mathrm{w,Q_0}}}{D_{\mathrm{c,Q_0}}}\right)^{-1} \,. \tag{2.3}$$

Usually, Q_0 is the beam quality specifier for a ^{60}Co gamma beam.

The direct measurement of p_{Q} and $k_{\mathrm{Q,Q_0}}$ is a challenging task. On the other hand, their calculation via Monte Carlo simulation is easier and more readily available, by determining $D_{\mathrm{w,Q}}$, $D_{\mathrm{c,Q}}$ and $(s_{\mathrm{w,air}})_{\mathrm{Q}}$ and using equations (4.1) and (4.2). Of course this computational approach will be feasible only if the ionization chambers can be modeled with enough accuracy. Alternatively, Sempau *et al.* [3] suggested to calculate $k_{\mathrm{Q,Q_0}}$ as

$$k_{\mathrm{Q,Q_0}} \;=\; \frac{f_{\mathrm{c,Q}}}{f_{\mathrm{c,Q_0}}} \,, \tag{2.4}$$

where $f_{\mathrm{c,Q}}$ is an overall ionization chamber and quality dependent factor that relates the absorbed dose in the medium with the absorbed dose in the detector:

$$D_{\mathrm{w,Q}} \;=\; D_{\mathrm{c,Q}} \cdot f_{\mathrm{c,Q}} \,. \tag{2.5}$$

Comparing this equation with (4.1) one can say that, formally, the factor $f_{c,Q}$ could be identified with the product $p_Q \cdot (s_{w,air})_Q$. However, the calculation of this last product is based on various approximations [3]: the electron fluence in the medium is the same as in the real detector, the various perturbation effects included in p_Q are independent and the stopping-power ratios and the perturbation effects are uncorrelated. The direct calculation of $f_{c,Q}$ does not require these assumptions. In fact, this factor could be understood as a modified stopping-power ratio which is calculated using the correct fluences in the medium and in the detector and taking into account in a realistic way the effect due to the fact that the detector is actually situated in the medium.

In this work we have calculated both p_Q and k_{Q,Q_0} for three ionization chambers, using the Monte Carlo simulation code PENELOPE [4]. Specifically we have analyzed the NE2571 Farmer-type chamber, manufactured by QADOS (Sandhurst, UK) and the A19 and A12S chambers, manufactured by Standard Imaging (Middleton, USA). The results obtained have been compared to those quoted in TRS-398 [2], with the results obtained in previous simulations done with the EGSnrc Monte Carlo code [5,6] and with measurements summarized in [7,8].

2.2. Material and methods

2.2.1. PENELOPE code

Nowadays, different general purpose Monte Carlo codes, such as PENELOPE [4], EGSnrc [9], Geant4 [10] and MCNPX [11], are able to model the geometry of ionization chambers with enough accuracy to permit a feasible comparison with measurements.

In this work we have used PENELOPE (v. 2008) [4]. This code permits to transport electrons and positrons within a mixed algorithm in which interaction events are classified as hard or soft. Hard events correspond to angular deflections or energy losses larger than threshold values defined by the user. These kind of events are simulated in a (detailed) analogue way, interaction by interaction. The combined effect of all soft events that occur between two hard collisions is simulated by means of an artificial single event, using a multiple scattering model. Detailed simulation is also used for photons.

In PENELOPE, the geometries of the ionization chambers can be built up by means of quadric surfaces through the package PENGEOM. Materials can be generated knowing their densities and stoichiometric composition or selected from an ample database. PENELOPE needs a main program to control the simulation process. In this work we have used penEasy [12]. This code is capable of solving a wide range of situations in Monte Carlo simulations, including those of interest in this work. In order to reduce the CPU time consumed in the simulations, we adapted clonEasy [13], a code which permits parallel simulation in various computers. All caculations were done on a LINUX cluster in which up to 20 CPU's could be used simultaneously.

The evaluation of Monte Carlo estimates and the corresponding statistical uncertainties was done according to [3,4].

PENELOPE transport parameters determine the average angular deflection between two consecutive hard elastic collisions (C_1, which is expressed in terms of the average cosine of the deflection angle), the maximum average fractional energy loss between consecutive hard elastic events (C_2) and the threshold energies for hard inelastic interactions ($W_{\rm cc}$) and hard bremsstrahlung emission ($W_{\rm cr}$) (see [4] for details). In addition, the absorption energies at which the track simulation is stopped and the parameter $s_{\rm max}$, which fixes the maximum step between interactions, must be defined. All these parameters should be established for each material in the geometry. In addition, absorption energies must be chosen for each particle type and each material.

In our simulations we used $C_1 = C_2 = 0.02$ in all regions except the water phantom and the air surrounding the geometry where $C_1 = C_2 = 0.1$ were fixed. On the other hand, $W_{\rm cc} = 0.01 \cdot E_{\rm max}$ and $W_{\rm cr} = 0.001 \cdot E_{\rm max}$, with $E_{\rm max}$ the maximum energy of the initial particles. For the absorption energies we used $E_{\rm abs}(e^-, e^+) = W_{\rm cc}$ and $E_{\rm abs}(\gamma) = W_{cr}$. We have checked that reducing the values of these parameters do not change the results of our simulations. Finally, $s_{\rm max}$ was set up, as suggested in the code user manual, to one tenth of the characteristic thickness of each material in the geometry.

2.2.2. Thimble ionization chambers

Three thimble type ionization chambers were studied in this work. The first one is the NE2571 Farmer-type chamber. The geometry details were obtained from the works of Aird and Farmer [14] and Wulff *et al.* [5]. Figure 2.1 shows a drawing of the approximated geometry used in the simulations. The chamber cavity has a diameter of 0.64 cm and a length of 2.40 cm and includes a central electrode made of aluminium and with a diameter of 0.1 cm. The graphite wall has a thickness of 0.04 cm. Additionally, the chamber model includes a sleeve of 0.10 cm made of PMMA (polymethyl methacrylate). The nominal chamber volume is 0.6 cm^3. An insulator made of PTFE (polytetrafluoroethylene) is between the electrode and the wall.

The other two ionization chambers studied are sketched in figure 3.1. These are the models A19 and A12S from Standard Imaging. The detailed geometries have been obtained from the manufacturer. The A19 has an air cavity with a diameter of 0.60 cm which includes a central electrode with a diameter of 0.10 cm. The air cavity volume is about 0.62 cm^3. The A12S has an air cavity volume of 0.25 cm^3 with a diameter of 0.60 cm and a central electrode with a diameter of 0.10 cm. These ionization chambers are made basically of C552 (an air-equivalent conductive plastic with a nominal density of 1.76 g cm^{-3}). In these geometries also the materials PTFE (polytetrafluoroethylene) and POM (polyoxymethylene) were used.

2.2.3. Simulation setup

The geometrical setup used in our simulations was constructed according to TRS-398 [2]. The ionization chamber was situated at the reference depth (5 cm in the case of the ^{60}Co source and 10 cm for the remaining MV photon sources), in the beam axis, inside a water phantom of $50 \times 50 \times 50$ cm^3. The source-to-surface distance was 100 cm and the beams were collimated to produce a radiation field of 10×10 cm^2 at the surface of the phantom. The dose scored within the active volume of the chamber provided us $D_{c,Q}$.

To obtain $D_{w,Q}$, we scored the dose in a finite small volume of water placed at the reference point. Following Kawrakow [15], we used a cylinder with a radius of 1 cm and 0.025 cm high. For comparison, we performed a calculation, for the ^{60}Co gamma beam, using a cylindrical scoring voxel with a radius of 0.5 cm and $3 \cdot 10^{-4}$ cm high, which is the same considered by Panettieri *et al.* [16]. The results obtained in this way differed less than 0.06 % from those found with the larger scoring voxels.

The overall perturbation factor p_Q was calculated according to equation (4.1). The necessary data for the stopping power ratios $(s_{w,air})_Q$ were taken from [2,17]. On the other hand, the factor $f_{c,Q}$ was evaluated from equation (4.4). The values obtained were used to calculate k_{Q,Q_0}, following equation (4.3).

The results obtained for the global perturbation factor p_Q were linearly fitted using a function

$$f(x) = a\,x + b\,. \tag{2.6}$$

The results obtained for k_{Q,Q_0} were fitted using a sigmoid function

$$f(x) = s\left(1 - \exp\left[\frac{x - t}{u}\right]\right)\,. \tag{2.7}$$

In this fitting functions x stands for TPR^{20}_{10}.

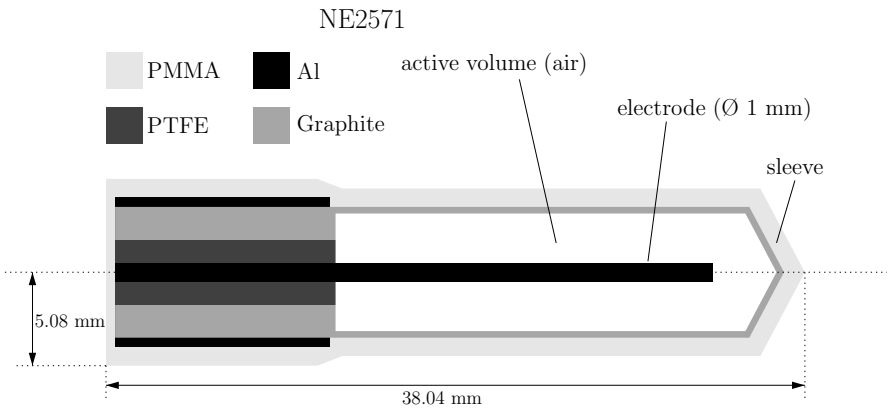

Figura 2.1: Scheme of the approximate geometry of the NE2571 ionization chamber used in our simulations.

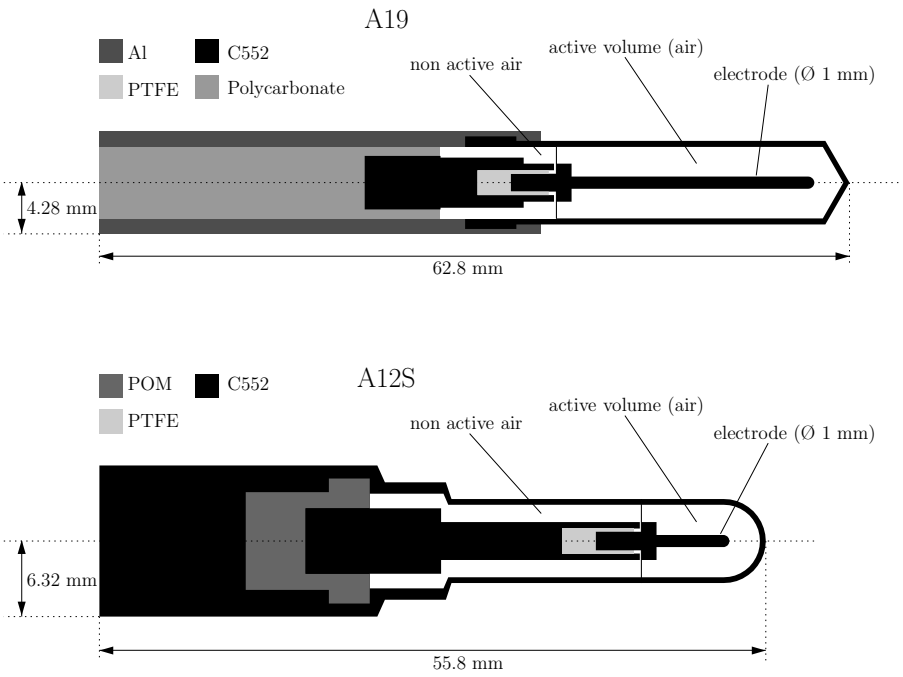

Figura 2.2: Scheme of the geometry of the A19 and A12S ionization chambers used in our simulations. These chambers have not sleeve because they are water tight.

2.2.4. Uncertainties

Simulations were performed by following a number of particles enough to have statistical uncertainties below 0.01 % (with a coverage factor $k = 2$) in the depth doses calculated. The number of histories simulated ranged between $3 \cdot 10^9$ for the largest chambers (NE2571 and A19) and the spectrum with a lower energy (^{60}Co) and $2 \cdot 10^{10}$ for the smaller chamber (A12S) and the spectrum with a larger energy (Elekta SL25 at 25 MV).

Apart from these, systematic uncertainties were considered according to the recent results of Wulff *et al.* [18] and Muir and Rogers [6] concerning k_{Q,Q_0}. The first authors found that electron cross sections were the largest source of systematic uncertainties in this kind of calculations. For the NE2571 chamber, they quoted values ranging from 0.2 %, for 6MV sources, to 0.4 %, for 24 MV sources. On the other hand, Muir and Rogers obtained that the largest sources of type B uncertainties were the assumption of a constant average energy lost per Coulomb of charge released by electrons in air and the uncertainty in the cross-section for photons in water. Considering various types of calculations, they obtained maximum relative uncertainties of 0.43 % (for the NE2571 chamber) and 0.49 % (for chambers like A19 and A12S), though they did not study the variation with the source energy. These authors did not evaluate the uncertainties in p_Q factors.

Despite the differences in the approaches considered by these authors to analyze the systematic uncertainties, their results were comparable. Thus we have assumed the values they quoted as a conservative estimate of these uncertainties in our calculations. Specifically, in the results shown below, type B uncertainties in k_{Q,Q_0} have been included as indicated by Wulff *et al.* [18] in the case of the NE2571 ionization chamber, assuming a

linear dependence with the energy of the source. On the other hand, and following the results of Muir and Rogers [6], we have considered a slightly larger range (up to 0.5 %) in case of A19 and A12S chambers.

2.2.5. Radiation sources

In this work we used a ^{60}Co gamma beam, whose spectrum was obtained from the work of Mora and Maio [19], and various photon beams corresponding to different linear accelerators. In particular we considered a Varian Clinac LE of 4 MV, a Varian Clinac HE of 6, 10, 15 and 18 MV, a Siemens KD of 6 and 18 MV and an Elekta SL25 of 6 and 25 MV. The photon spectra of these accelerators were taken from Sheikh-Bagheri and Rogers [20].

In all the simulations, sources were assumed to be point sources emitting photons with the corresponding spectrum. As indicated, particle transport was performed with the Monte Carlo code PENELOPE [4]. It is worth to mention that Wulff *et al.* [5] did not find significant differences in the calculated quality indexes when full beam Monte Carlo models of the 6 and 18 MV Siemens KD linacs were used to perform the calculations instead a point source with the adequate photon spectrum.

Using the geometrical setup described above, depth doses in the water phantom were calculated. These calculations were performed using cylindrical scoring voxels centered in the beam axis, with a radius of 0.5 cm and a height of 0.2 cm, which are the same as those considered by Muir and Rogers [6]. This permitted us to determine the quality index, TPR_{10}^{20}, for the various beams considered. This index is given by the ratio of the dose absorbed in water at depths of 20 and 10 cm, with a distance between the source and the measurement depths of 100 cm and a field at these depths of 10 cm × 10 cm. Instead we calculate TPR_{10}^{20} according to [2,21]

$$\mathrm{TPR}_{10}^{20} = 1.2661 \cdot \mathrm{PDD}_{10}^{20} - 0.0595\,, \tag{2.8}$$

where PDD_{10}^{20} is the ratio of the percent depth-doses at 20 cm and 10 cm depths for a field size of 10 cm x 10 cm defined at the phantom surface with an source-to-surface distance of 100 cm. According to Followill *et al.* [21], this approach introduces an uncertainty of ± 0.01 (with a coverage factor $k = 2$) in the calculation of TPR_{10}^{20}.

2.3. Results and discussion

2.3.1. Values of TPR_{10}^{20}

The results obtained for TPR_{10}^{20} are shown in table 4.2 where they are compared to the results of Wulff *et al.* [5] and Muir and Rogers [6]. We calculated TPR_{10}^{20} values using equation (2.8). Wulff *et al.* performed a direct calculation of this quality index, using

Tabla 2.1: Comparison of the quality indexes TPR_{10}^{20} obtained in this work, using equation (2.8), with those of Wulff et al. [5] and Muir and Rogers [6], calculated with equation (2.9), for the various radiation sources considered. The uncertainty in our calculation is estimated in ± 0.01 *(with a coverage factor* $k = 2$*). The values of Wulff et al. have a statiscal uncertainty below 0.2 %. Those of Muir and Rogers show a maximum deviation of 0.007. The values between parentheses give the relative differences in absolute value with our results.*

		TPR_{10}^{20}		
source	energy [MV]	this work	Wulff *et al.* [5]	Muir and Rogers [6]
^{60}Co	-	0.571	0.572 (0.17 %)	0.569 (0.35 %)
Clinac LE	4	0.644	0.621 (3.57 %)	0.623 (3.26 %)
Clinac HE	6	0.670	0.662 (1.19 %)	0.666 (0.60 %)
	10	0.739	0.736 (0.41 %)	0.734 (0.68 %)
	15	0.763	0.755 (1.05 %)	0.763 (0.00 %)
	18	0.787	0.780 (0.89 %)	0.785 (0.25 %)
Siemens KD	6	0.679	0.676 (0.44 %)	0.671 (1.18 %)
	18	0.772	0.768 (0.52 %)	0.762 (1.30 %)
Elekta SL25	6	0.688	-	0.672 (2.38 %)
	25	0.799	0.797 (0.25 %)	0.791 (1.00 %)

the definition of the index given above. Muir and Rogers used the formula of Kalach and Rogers [24]

$$\mathrm{TPR}_{10}^{20} = -0.8228 + 0.0342 \cdot (\,\%\mathrm{dd}(10)_x) - 0.0001776 \cdot (\,\%\mathrm{dd}(10)_x)^2\,, \qquad (2.9)$$

where $\%\mathrm{dd}(10)_x$ is the photon component of the percent depth-dose at 10 cm depth in a 10×10 cm^2 field at the surface. This equation introduces a maximum deviation in TPR_{10}^{20} of 0.007.

The largest differences were found for the Clinac LE at 4 MV; we found 3.6 % and 3.3 % with respect to the values quoted by Wulff *et al.* and Muir and Rogers, respectively. This discrepancy contrasts with the correction factors,$k_{\mathrm{Q,Q_0}}$ and p_{Q}, found for this source which are within the general trend (see next section). In any case, if the uncertainties introduced by the use of equations (2.8) and (2.9) are taken into account the differences discussed are significantly reduced.

The relative differences found for the other radiation sources are similar to those existing between the results of Wulff *et al.* [5] and Muir and Rogers [6], both obtained with EGSnrc. It is worth to point out the overall agreement found with the results of Muir and Rogers for the Clinac HE.

2.3.2. Correction factors for the NE2571 ionization chamber

We first discuss the results obtained for the beam quality correction factor, $k_{\mathrm{Q,Q_0}}$ in case of the NE2571 ionization chamber. In the upper panel of figure 2.3, our results (open

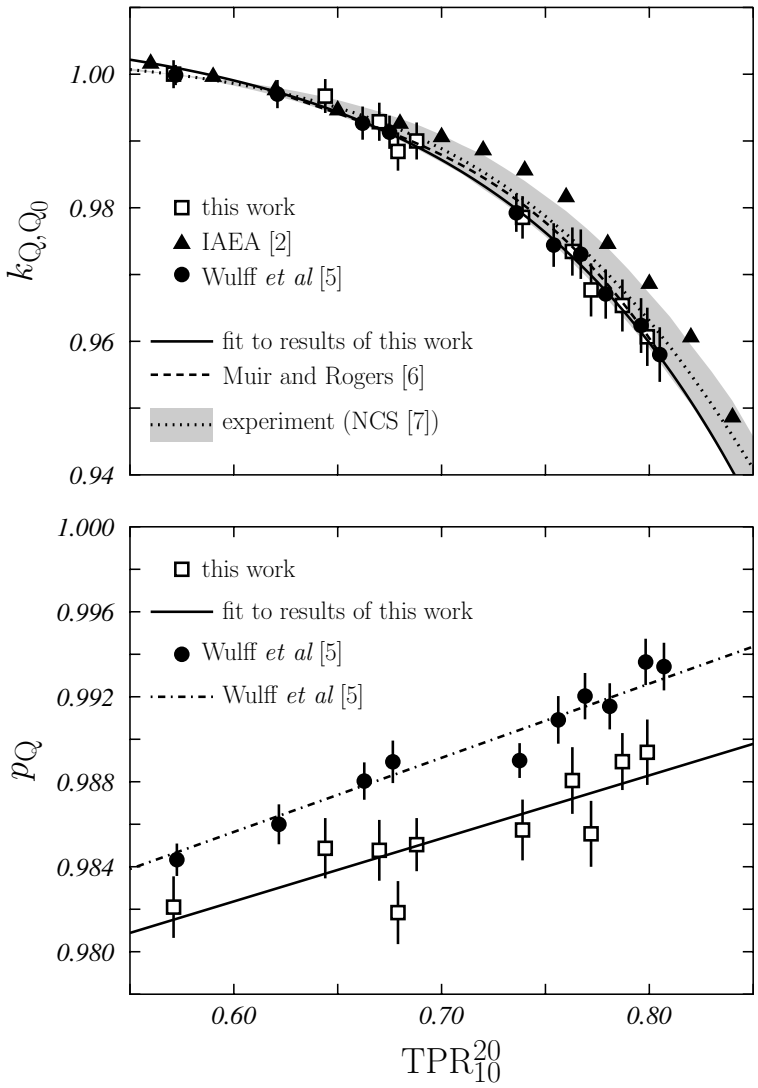

Figura 2.3: Beam quality correction factor, k_{Q,Q_0} (upper panel), and perturbation factor, p_Q (lower panel), for the NE2571 ionization chamber, as a function of the beam quality index TPR_{10}^{20}. Open squares represent the results obtained in this work and solid circles those of Wulff et al. [5]. Uncertainties are given with a coverage factor $k = 1$. Systematic uncertainties are included for k_{Q,Q_0} in both our results and those of Wulff et al. (see text). In the upper panel, solid triangles show the values quoted in TRS-398 [2], the dashed curve is the fit to their Monte Carlo results quoted by Muir and Rogers [6]. The solid curve corresponds to a fit to the results we have obtained using the fitting function defined in equation (4.5) with $s = 1.008(4)$, $t = 1.16(5)$ and $u = 0.12(2)$. The dotted line represents the fit to the experimental data done in [7] and the gray area indicates the range of variation of this fit with a coverage factor $k = 1$. In the lower panel the solid line corresponds to a fit to the results we have obtained using the function (4.11). In this case $a = 0.030(7)$ and $b = 0.965(5)$. Dashed-dotted line corresponds to the linear fit quoted by Wulff et al. (2008). The number in parentheses represents the statistical uncertainty, e.g. 1.008(4) means 1.008 ± 0.004 ($k = 1$).

squares) are compared to those of Wulff *et al.* [5], which are shown with solid circles, and also with those quoted in TRS-398 protocol [2], plotted with solid triangles. The solid curve shows the fit to our results using the function defined in equation (4.5). The dashed curve represents the fit quoted by Muir and Rogers [6] to their EGSnrc Monte Carlo results. The dotted line represents the fit to the experimental data done in [7] and the gray area shows the range of variation of this fit.

Our results agree rather well with those of Wulff *et al.* [5]. On the other hand, they differ significantly from those of TRS-398. The fit to our data (solid curve) and that quoted by Muir and Rogers [6] (dahsed curve) also show a good agreement, despite the differences discussed above between the respective calculations in the TPR_{10}^{20} values (see table 4.2). There is also an overall agreement with the fit to experimental data of [7].

In the lower panel of figure 2.3, the overall perturbation factors p_{Q} we have obtained are plotted with open squares. Solid line gives the linear fit of these results. For comparison we show, with solid circles, the values quoted by Wulff *et al.* [5] together with the linear fit given by these authors. The results differ significantly for the reference quality (^{60}Co). Therein a relative difference of $\sim 0.4\,\%$ is found and this difference grows slightly as TPR_{10}^{20} increases. In fact, both sets of values show an almost parallel behavior: the slope quoted by Wulff *et al.* is 0.0349 while we have found 0.030 ± 0.007. This discrepancy between EGSnrc and PENELOPE calculations is of the same order of that found by Wulff and Zink for the NACP-02 chamber in case of ^{60}Co beams [22]. These authors quoted $0.3\,\%$ overall deviation for the p_{Q} correction factor. Our results point out a systematic difference between both codes in what refers to this factor p_{Q}.

It should be noted that the result obtained for the Siemens KD at 6 MV ($\mathrm{TPR}_{10}^{20} = 0.679$) is clearly out of the trend defined by the rest of the radiation sources investigated. This does not appear so clearly in the case of $k_{\mathrm{Q,Q_0}}$ (upper panel) and did not show up in the results quoted in table 4.2 where differences of $0.44\,\%$ with Wulff *et al.* [5] and $1.18\,\%$ with Muir and Rogers [6] were found. Recently, Muir *et al.* [23] have found a outlier behavior when they calculated differences in the $k_{\mathrm{Q,Q_0}}$ factors for the NE2571, the PTW30012 and the IBA FC-65G ionization chambers when the spectrum of the Siemens KD operating at 18 MV was considered. This result together with that we have found for 6MV could indicate a problem with the published spectra for the Siemens KD linac. A similar situation can be observed in the results of Wulff *et al.* [5] for the Varian Clinac HE at 10 MV ($\mathrm{TPR}_{10}^{20} = 0.736$): in that case the value for p_{Q} lies well below the linear trend (dashed dotted line).

2.3.3. Correction factors for A19 and A12S ionization chambers

Now we discuss the results obtained for the beam quality correction factor, $k_{\mathrm{Q,Q_0}}$, for the Standard Imaging A19 and A12S thimble ionization chambers. Results are shown in figure 2.4 with open squares. Also we show with solid curves the fits to data using the function in equation (4.5). These results are compared to the measurements of McEwen [8] (solid circles) and with the fits to their Monte Carlo results quoted by Muir and Rogers [6] (dashed curve).

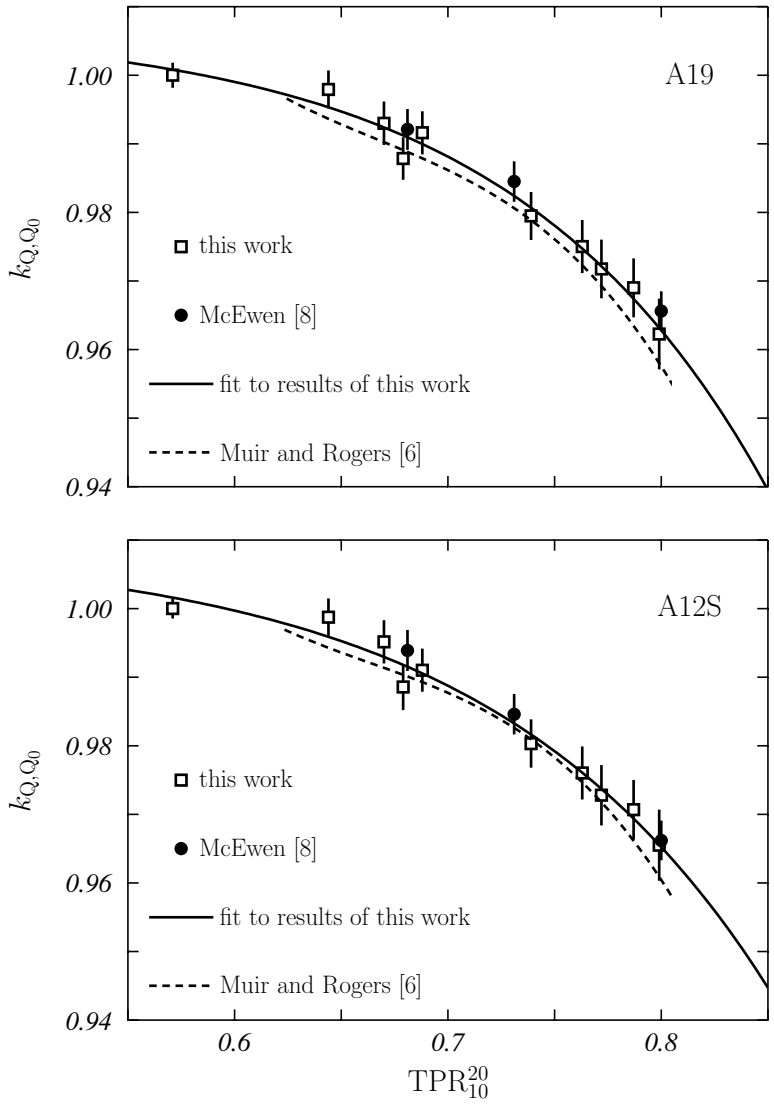

Figura 2.4: Beam quality correction factor, k_{Q,Q_0} for A19 (upper panel) and A12S (lower panel) ionization chambers, as a function of the beam quality index TPR_{10}^{20}. *Open squares correspond to the results we have obtained. Uncertainties are given with a coverage factor $k = 1$. Systematic uncertainties are included (see text). Solid curves correspond to fits to the results we have obtained. The fitting function defined in equation (4.5) was used. For the A19 chamber, $s = 1.007(5)$, $t = 1.17(8)$ and $u = 0.12(3)$. For the A12S chamber, $s = 1.117(6)$, $t = 1.21(9)$ and $u = 0.13(3)$. Here, the number in parentheses represents the statistical uncertainty, e.g. 1.21(9) means 1.21 ± 0.09 ($k = 1$). Dashed curves are the fits to their Monte Carlo results quoted by Muir and Rogers [6].*

Our results show a reasonable agreement with the fits of Muir and Rogers [6] and with the experimental measurements of McEwen [8]. PENELOPE results seem to be in better agreement with experiment than EGSnrc ones at the higher energies. The same occurs for both chambers. The results shown here, together with those of figure 2.3 (upper panel) indicate that the function (4.5) permits a good description of the k_{Q,Q_0} data. It is worth

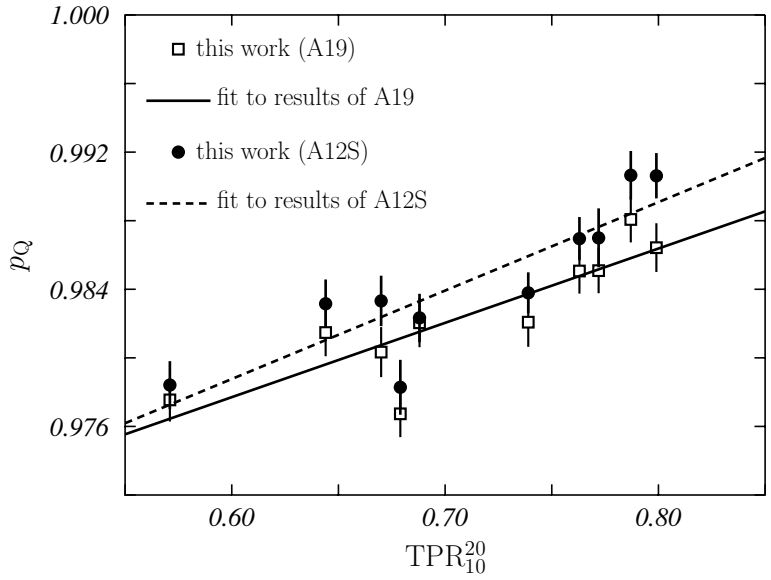

Figura 2.5: Perturbation factor, p_Q, for the A19 (open squares) and A12S (solid circles) ionization chambers, as a function of beam quality index TPR_{10}^{20}*. Uncertainties are given at 2σ level. The lines are linear fits to the results we have obtained for the two chambers. The function (4.11) has been used. For the A19 chamber the fitting parameters were* $a = 0.065(7)$ *and* $b = 0.939(5)$*. In the case of the A12S chamber,* $a = 0.065(7)$ *and* $b = 0.941(5)$*. Here, the number in parentheses represents the statistical uncertainty at 1σ level, e.g. 0.939(5) means* 0.939 ± 0.005.

to point out that, as indicated in [7], sigmoid fits preserve their smooth shape even when noisy data are considered. This does not happens in general with polynomial fits.

Figure 2.5 shows the results obtained for the global perturbation factor p_Q for the A19 (open squares) and A12S (solid circles) chambers, together with the respective linear fits. These linear fits show up as slightly divergent when TPR_{10}^{20} increases. The values obtained for $TPR_{10}^{20} = 0.679$, which correspond to the Siemens KD at 6 MV (see table 4.2), are those showing a larger disagreement with the general trend provided by the fits. This was also observed in the case of the k_{Q,Q_0} quality correction factor, also in both chambers (see figure 2.4). And in the case of the NE2571 chamber (see figure 2.3) the value of p_Q found for this beam is also out of trend, while for k_{Q,Q_0} the behavior is reasonable. This could indicate that there is some problem with the spectrum of the corresponding beam that we have not been able to identify yet.

2.4. Conclusions

In this work, the perturbation factors for the NE2571 ionization chamber, which is widely used in radioteraphy dosimetry, have been calculated using the Monte Carlo code PENELOPE.

The values of k_{Q,Q_0} that we have obtained are in good agreement with those quoted by Wulff *et al.* [5] and Muir and Rogers [6], which were obtained with the code EGSnrc

and differ significantly from those of TRS-398 protocol [2]. Also an overall agreement with the experimental data summarized in [7] has been found.

The overall perturbation factor p_{Q} obtained by Wulff *et al.* with EGSnrc [5] differs from that we have found with PENELOPE by $\sim 0.4\,\%$ for the ^{60}Co beam. With increasing TPR_{10}^{20} the results of both calculations behave almost parallel.

The same perturbation factors have been calculated for the Standard Imaging A19 and A12S ionization chambers. A reasonable agreement with the Monte Carlo results found by Muir and Rogers [6] with EGSnrc and with the measurements of McEwen [8] has been found for both ionization chambers.

Acknowledgements

The authors thanks Brian Hooten, from Standard Imaging, for providing us with the geometries of the ionization chambers studied. This work has been supported in part by the Junta de Andalucía (FQM0220) and by the Spanish DGI (FPA2009-14091-C02-02).

[1] Almond PR, Biggs PJ, Caursey BM, Hanson WF, Saiful HM, Nat R, Rogers DWO. AAPM's TG-51 protocol for clinical reference dosimetry of high-energy photon and electron beams. Med Phys 1999; 26: 1847-70.

[2] International Atomic Energy Agency. Absorbed dose determination in external beam radiotherapy, IAEA Technical Reports Series 398. Vienna: IAEA; 2000.

[3] Sempau J, Andreo P, Aldana J, Mazurier J, Salvat F. Electron beam quality correction factors for plane-parallel ionization chambers in high energy photon beams: Monte Carlo calculations using the PENELOPE system. Phys Med Biol 2004; 49: 4427-44.

[4] Salvat F, Fernández-Varea JM, Sempau J. PENELOPE: a code system for Monte Carlo simulation of electron and photon transport. Paris: Nuclear Energy Agency; 2008.

[5] Wulff J, Heverhagen JT, Zink K. Monte Carlo based perturbation and beam quality corrections factors for thimble ionization chambers in high energy photon beams. Phys Med Biol 2008; 53: 2823-36.

[6] Muir BR, Rogers DWO. Monte Carlo calculations of k_Q, the beam quality conversion factor. Med Phys 2010; 37: 5939-50.

[7] Nederlandse Commissie voor Stralingsdosimetrie. Code of practice for the absorbed dose determination in high energy photon and electron beams. NCS Report 18. Delft: NCS; 2008.

[8] McEwen MR. Measurement of ionization chamber absorbed dose kQ factors in megavoltage photon beams. Med. Phys. 2010; 37: 2179-93.

[9] Kawrakow I, Rogers DWO. The EGSnrc code system: Monte Carlo simulation of electron and photon transport. NRC Technical Report No. PIRS-701, v4-2-2-5. Ottawa: National Research Council of Canada; 2007;
see http://www.irs.inms.nrc.ca/inms/irs/EGSnrc/EGSnrc.html.

[10] Agostinelli S, Allison J, Amako K, Apostolakis J, *et al.* Geant4–a simulation tool kit. Nucl. Instr. Meth. Phys. Res. A 2003; 506: 250-303.

[11] Pelowitz DB, ed. MCNPX UserÕs Manual version 2.5.0, Report LA-UR-02-2607. Los Alamos: Los Alamos National Laboratory; 2005.

[12] Sempau J. penEasy: A modular main program and voxelized geometry package for PENELOPE. www.upc.edu/inte/downloads/penEasy.htm; 2009.

[13] Badal A, Sempau J. clonEasy: A package of linux scripts for the parallelization of Monte Carlo simulations. Comp Phys Comm 2005; 175: 440-50.

[14] Aird EG, Farmer FT. The design of a thimble chamber for the Farmer dosemeter. Phys Med Biol 1972; 17: 169-74.

[15] Kawrakow I. On the effective point of measurement in megavoltage photon beams. Med Phys 2006; 33: 1829-39

[16] Panettieri V, Sempau J, Andreo P. Chamber-quality factors in ^{60}Co for three plane parallel chambers for the dosimetry of electrons, protons and heavy charged particles: PENELOPE Monte Carlo simulations. Phys Med Biol 2008; 53: 5917-26.

[17] Andreo P. Improved calculations of stopping-power ratios and their correlation with the quality of therapeutic photon beams. Proceedings Symposium on Measurement Assurance in Dosimetry. IAEA, Vienna: IAEA; 1994.

[18] Wulff J, Heverhagen JT, Zink K, Kawrakow I. Investigation of systematic uncertainties in Monte Carlo-calculated beam quality correction factors. Phys Med Biol 2010; 55: 4481-93.

[19] Mora GM, Maio A. Monte Carlo simulation of a typical ^{60}Co therapy source. Med Phys 1999; 26: 1847-70.

[20] Sheikh-Bagheri D, Rogers DWO. Monte Carlo calculation of nine megavoltage photon beam spectra using BEAM code. Med Phys 2002; 29: 391-402.

[21] Followill DS, Tailor RC, Tello VM, Hanson WF. An empirical relationship for determining photon beam quality in TG-21 from a ratio of percent depth doses. Med Phys 1998; 25: 1202-5.

[22] Wulff J, Zink K. Chamber quality factors for the NACP-02 chamber in ^{60}Co beams: Comparison of EGSnrc and PENELOPE Monte Carlo simulations. International Symposium on Standards, Applications and Quality Assurance in Medical Radiation Dosimetry. IAEA, Vienna; 2010.

[23] Muir BR, McEwen MR, Rogers DWO. Measured and Monte Carlo calculated kQ factors: Accuracy and comparison. Med Phys 2011; 38: 4600-9.

[24] Kalach NI, Rogers DWO. Which accelerator photon beams are ÔclinicalikeÕ for reference dosimetry purposes? Med Phys 2003; 30:1546-55.

Capítulo 3

Cámaras plano-paralelas

Physics in Medicine and Biology 59 (2014) 6673-6691

Electron beam quality k_{Q,Q_0} factors for various ionization chambers: A Monte Carlo investigation with PENELOPE

F. Erazo[1,2,3], L. Brualla[4] and A.M. Lallena[1]

[1] Departamento de Física Atómica, Molecular y Nuclear, Universidad de Granada, E-18071 Granada, Spain
[2] Instituto del Cáncer - SOLCA, Cuenca, Ecuador
[3] Escuela de Tecnología Médica, Facultad de Medicina, Universidad de Cuenca, Cuenca, Ecuador
[4] NCTeam, Strahlenklinik, Universitätsklinikum Essen, Hufelandstraße 55, D-45122 Essen, Germany

In this work we calculate the beam quality correction factor k_{Q,Q_0} for various plane-parallel ionization chambers. A set of Monte Carlo calculations using the code PENELOPE/penEasy have been carried out to calculate the overall correction factor $f_{c,Q}$ for eight electron beams corresponding to a Varian Clinac 2100 C/D, with nominal energies ranging between 6 and 22 MeV, for a ^{60}Co beam, that has been used as the reference quality Q_0, and also for eight monoenergetic electron beams reproducing the quality index R_{50} of the Clinac beams. Two field sizes, 10×10 cm^2 and 20×20 cm^2 have been considered. The k_{Q,Q_0} factors have been calculated as the ratio between $f_{c,Q}$ and f_{c,Q_0}. Values for the Exradin A10, A11, A11TW, P11, P11TW, T11 and T11TW ionization chambers, manufactured by Standard Imaging, as well as for the NACP-02 have been obtained. The results found with the Clinac beams for the two field sizes analyzed show differences below 0.6 %, even in the case of the higher energy electron beams. The k_{Q,Q_0} values obtained with the Clinac beams are 1 % larger than those found with the monoenergetic beams for the higher energies, above 12 MeV. This difference can be ascribed to secondary photons produced in the linac head and the air path towards the phantom. Contrary to what was quoted in a previous work [*Phys. Med. Biol.* **49** 4427-4444 (2004)], the beam quality correction factors obtained with the complete Clinac geometries and with the monoenergetic beams differ significantly for energies above 12 MeV. Material differences existing between chambers that have the same geometry produce non-negligible modifications in the value of these correction factors.

3.1. Introduction

Both TG-51 (Almond *et al.* 1999) and TRS-398 (IAEA 2000) protocols use standards based on water to evaluate absorbed doses. According to the Bragg-Gray theory, the absorbed dose at a point in water, $D_{\mathrm{w,Q}}$, for a certain beam quality Q, can be related to the mean absorbed dose in an air cavity, $D_{\mathrm{air,Q}}$, as

$$D_{\mathrm{w,Q}} \;=\; D_{\mathrm{air,Q}}\,(S_{\mathrm{w,air}})_{\mathrm{Q}}\,, \tag{3.1}$$

where $(S_{\mathrm{w,air}})_{\mathrm{Q}}$ is the stopping power ratio between water and air (Nahum 1978, Siebers *et al.* 2000, Jang *et al.* 2007, Fernández-Varea *et al.* 2007). In this expression it is assumed that the presence of the ideal detector does not modify the electron fluence at the measuring point in the medium. In general, a real detector, e.g. a plane parallel ionization chamber, shows some deviations from the ideal detector considered in the theory and a factor, $p_{\mathrm{c,Q}}$, must be included to account for these deviations:

$$D_{\mathrm{w,Q}} \;=\; D_{\mathrm{air,Q}}\,p_{\mathrm{c,Q}}\,(S_{\mathrm{w,air}})_{\mathrm{Q}}\,. \tag{3.2}$$

Here $p_{\mathrm{c,Q}}$ is named as a "perturbation" factor because it takes into account the fact that the electron fluence at the measuring position in the water medium is perturbed by the presence of the detector. It can be factorized in terms of individual correction factors, assumed to be independent from each other and uncorrelated among them, that take into account the various effects produced by the detector (IAEA 2000): (i) the in-scattering of electrons that changes the electron fluence inside a cavity with respect to that in the water medium in absence of the cavity; (ii) the fact that detector wall material, and that of any waterproof sleeve present, is different from water; (iii) the effect on the chamber response of the central electrode during in-phantom measurements in high energy particle beams, and (iv) the effect due to the replacement of a water volume with the detector cavity when the reference point is assumed at the chamber center (not required for plane-parallel ionization chambers).

The previous equation imposes a series of requirements that are difficult to fulfill. Apart from the necessary constancy of the electron fluence at the measuring point with and without the detector, it must be assumed that $p_{\mathrm{c,Q}}$ and $(S_{\mathrm{w,air}})_{\mathrm{Q}}$ are uncorrelated. Some authors (Sempau *et al.* 2004, Capote *et al.* 2004) proposed an alternative expression in which $D_{\mathrm{w,Q}}$ is related directly to the absorbed dose in the air cavity of the real detector $D_{\mathrm{c,Q}}$:

$$D_{\mathrm{w,Q}} \;=\; D_{\mathrm{c,Q}}\,f_{\mathrm{c,Q}}\,. \tag{3.3}$$

The obvious advantage is that the overall perturbation factor $f_{\mathrm{c,Q}}$ can be calculated using a realistic description of the geometry of the detector. The overall perturbation factor takes care in a direct way of the complete effect produced by the presence of the detector in the medium.

Ideally, reference laboratories should have the same beam quality Q than the user. In that case, the absorbed dose to water, at the reference depth z_{ref} in water, and in the absence of the chamber is given by (IAEA 2000)

$$D_{\mathrm{w,Q}} \;=\; M_{\mathrm{Q}}\,N_{D,\mathrm{w,Q}}\,, \tag{3.4}$$

where M_{Q} is the reading of the ionization chamber, corrected for the temperature, pressure, electrometer calibration, polarity effect and ion recombination, and $N_{D,\mathrm{w,Q}}$ is the calibration factor in terms of absorbed dose to water for the ionization chamber at the quality Q. However, reference laboratories usually calibrate the detector to a given calibration quality Q_0 and equation (3.4) must be written as

$$D_{\mathrm{w,Q}} \,=\, M_{\mathrm{Q}}\, N_{D,\mathrm{w},\mathrm{Q}_0}\, k_{\mathrm{Q},\mathrm{Q}_0}\,, \tag{3.5}$$

where $N_{D,\mathrm{w},\mathrm{Q}_0}$ is the calibration factor at the reference quality Q_0 and $k_{\mathrm{Q},\mathrm{Q}_0}$ is a chamber-specific factor that takes into account the differences between the beam quality Q_0 used in the chamber calibration and the beam quality Q available for the user. Usually a ^{60}Co gamma beam is considered as the Q_0 reference quality.

According to the works of Sempau *et al.* (2004) and Capote *et al.* (2004) the beam quality correction factor can be calculated as

$$k_{\mathrm{Q},\mathrm{Q}_0} \,=\, \frac{f_{\mathrm{c,Q}}}{f_{\mathrm{c},\mathrm{Q}_0}}\,, \tag{3.6}$$

an expression that has been widely used for different chambers and radiation sources (Zink and Wulff 2008, González-Castaño *et al.* 2009, Muir and Rogers 2010, Muir and Rogers 2013, Erazo and Lallena 2013). The previous equation is based on the assumption that $(W/e)_{\mathrm{air}}$, the average energy lost per unit charge released by electrons stopped in air, is independent of the beam energy. According to Svensson and Brahme (1986) it may vary 0.5 eV (1.5 %) with respect to ^{60}Co, for electron energies ranging between 0 and 40 MeV. This introduces an uncertainty in calculated $k_{\mathrm{Q},\mathrm{Q}_0}$ of about 0.5 % (Muir and Rogers 2013).

The aim of the present work is to calculate the correction factor $k_{\mathrm{Q},\mathrm{Q}_0}$ for seven Exradin plane-parallel ionization chambers using the Monte Carlo radiation transport code PENELOPE (Salvat *et al.* 2011). Eight electron beams, of nominal energies between 6 and 22 MeV, corresponding to a Varian Clinac 2100 C/D (Varian Medical Systems, Palo Alto, USA) are considered.

Sempau *et al.* (2004) found that the perturbation factors $f_{\mathrm{c,Q}}$ obtained for the NACP-02, PPC-05 and PPC-40 ionization chambers coincide when they are irradiated with a beam generated with a complete linac head model and with a monoenergetic beam having the same R_{50}. We check if this also occurs for the seven Exradin chambers under study. To do that, we consider several monoenergetic electron beams that reproduce the R_{50} of the Clinac beams mentioned. For comparison with the work of Sempau *et al.* (2004), the correction factor is also determined for the NACP-02 ionization chamber and the same radiation sources. The effect of the irradiation field size is studied by comparing the results obtained for fields of 10×10 cm^2 and 20×20 cm^2. Finally, and taking advantage of the fact that some of the chambers under study share the same geometry, the effect of the different materials conforming some of the elements of that geometries is also analyzed.

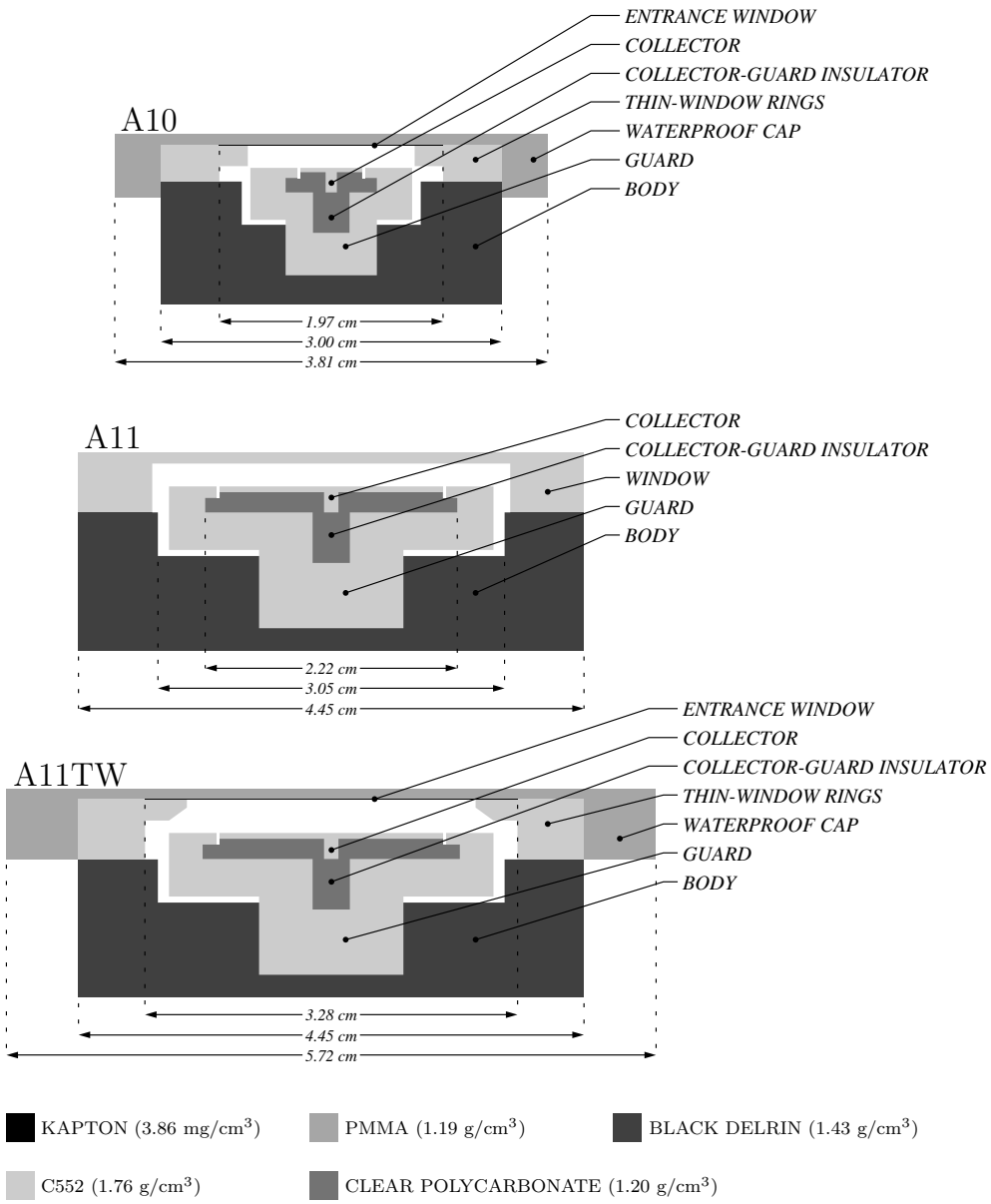

Figura 3.1: Scheme of the geometry of the Exradin ionization chambers A10, A11 and A11TW considered in our simulations. A11, P11 and T11 chambers have the same geometry. The same occurs for A11TW, P11TW and T11TW. The only differences are changes in some of the materials (see text for details.)

3.2. Material and methods

3.2.1. Ionization chambers

The Exradin ionization chambers A10, A11, A11TW, P11, P11TW, T11 and T11TW manufactured by Standard Imaging (Middleton, USA) were studied. Three of these chambers (A11TW, P11TW and T11TW) have an active volume of 0.92 cm^3; other three (A11,

P11 and T11) have a smaller volume of 0.62 cm^3, and, finally, the A10 chamber is much smaller than the other ones with a volume of 0.051 cm^3. Detailed chamber models were considered in dose to air cavity simulation including dimensions and materials provided by the manufacturer. Schemes of the A10, A11 and A11TW chambers are drawn in figure 3.1. The ionization chambers A11, P11 and T11 have the same geometry; the same happens with the A11TW, P11TW and T11TW chambers. The only difference is in the material conforming the collector, the guard, the thin-windows rings and the window (see figure3.1). The air equivalent plastic C552 used in the A11 and A11TW chambers in those elements of the geometry is substituted by polystyrene equivalent plastic D400 (with density 1.16 g/cm^3) in the P11 and P11TW chambers, and by tissue equivalent plastic A150 (with density 1.13 g/cm^3) in the T11 and T11TW chambers. C552 is also employed in the case of the A10 chamber.

As indicated in the Introduction the NACP-02 ionization chamber has been also studied. Figure 3.2 shows the geometry of the NACP-02 chamber considered in our simulations, which has been taken from the work of Williams *et al.* (1998). The active volume of this chamber (plotted with a square in the figure) is 0.157 cm^3.

The correction factors k_{Q,Q_0} were calculated for these chambers using equation (4.3). The $f_{c,Q}$ perturbation factor was obtained from equation (3.3). The absorbed doses at the medium, $D_{w,Q}$, and the detector, $D_{c,Q}$, were calculated in a series of Monte Carlo simulations run with the main program penEasy (Sempau 2009). This code is a main steering program that uses the penelope system (Salvat *et al.* 2011).

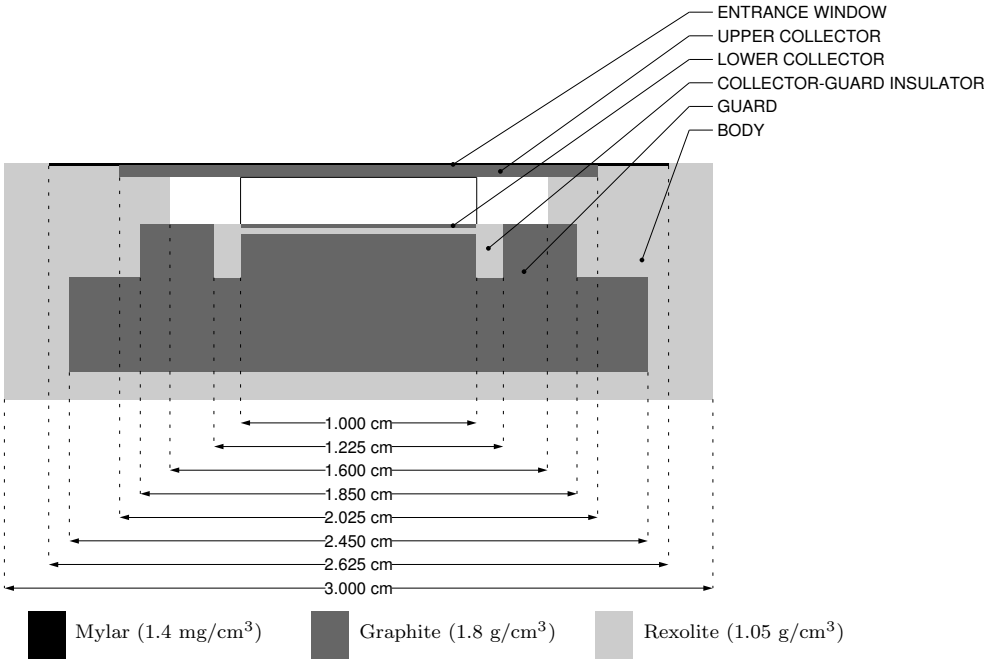

Figura 3.2: Scheme of the geometry of the NACP-02 ionization chamber considered in our simulations. The rectangle indicates the active volume.

3.2.2. Monte Carlo code PENELOPE

PENELOPE is a Monte Carlo general-purpose code that simulates the coupled transport of photons, electrons and positrons in matter, makes a good description of the particle transport trough the material interfaces and provides very good accuracy at low energies (Sempau *et al.* 2003, Faddegon *et al.* 2008, Faddegon *et al.* 2009, Salvat and Fernández-Varea 2009, Vilches *et al.* 2009). The capabilities of the code when simulating ionization chamber responses have been previously studied (Sempau and Andreo 2006,Yi *et al.* 2006).

Photons are transported within the conventional detailed method, in which all the interaction events are described in sequential order. Electrons and positrons are simulated using a mixed scheme where collisions are classified into hard and soft. Hard collisions are simulated, as photons, in a detailed way and are characterized by a polar deflection angle or energy loss above user-selectable threshold values. All soft interactions occurring between two consecutive hard collisions are described using a multiple scattering approximation. Electron and positron simulation is controlled by eight parameters: C_1, C_2, $W_{\rm CC}$, $W_{\rm CR}$, $E_{\rm ABS}(\gamma)$, $E_{\rm ABS}(\mathrm{e}^-)$, $E_{\rm ABS}(\mathrm{e}^+)$ and $s_{\rm max}$. C_1 is linked to the average angular deflection produced by all soft interactions occurred along a path length equal to the mean free path between consecutive hard elastic events. C_2 is the maximum average fractional energy loss between consecutive hard elastic events. $W_{\rm CC}$ and $W_{\rm CR}$ are cut-off energy values for hard inelastic collisions and bremsstrahlung emission, respectively. When the kinetic energy of a given particle becomes smaller than its corresponding $E_{\rm ABS}$, the simulation of this particle is stopped and the energy of the particle is deposited locally. Finally, $s_{\rm max}$ is the maximum length permitted to a simulation step.

In our simulations, we have followed the prescription of Sempau and Andreo (2006) who studied in a very detailed way the optimal values of the PENELOPE tracking parameters to simulate the response of ionization chambers. Specifically we have used $C_1 = C_2 = 0.02$ for all the materials forming the ionization chamber and a water volume extending 2 cm around it. For the rest of the materials in the simulation geometry we have fixed $C_1 = C_2 = 0.1$. We have used $E_{\rm ABS}(\mathrm{e}^-) = E_{\rm ABS}(\mathrm{e}^+) = 0.01\,E_{\rm max}$, $E_{\rm ABS}(\gamma) = 0.001\,E_{\rm max}$, with $E_{\rm max}$ the energy of the primary electrons at the source. The values of the parameter $s_{\rm max}$ have been fixed, as recommended in the code user manual (Salvat *et al.* 2011) to one tenth of the thickness of the corresponding material.

3.2.3. Radiation sources

We simulated the irradiation of the ionization chambers described above with beams of a Varian Clinac 2100 C/D with nominal electron energies of 6, 9, 12, 15, 16, 18, 20 and 22 MeV. The linac geometries were generated with the code PENEASYLINAC (Brualla *et al.* 2009, Sempau *et al.* 2011). This is a code that generates the necessary input files for the simulation with PENELOPE of most Varian linacs according to the Monte Carlo package distributed by this company. The code requires as input the type of linac used, the irradiation mode (electron or photon), the nominal energy of the beam, the field size, and the type and position of additional collimation devices such as multileaf collimators

Tabla 3.1: Energy E_{ini} of primary electrons used in the simulation of the Varian Clinac 2100 C/D, Bremsstrahlung tail calculated as the percentage of the maximum depth dose in the beam axis, and values of R_{50} found in these simulations for the different nominal energies considered. The R_{50} values obtained for the corresponding monoenergetic beams are shown for comparison. These results were obtained for a 10×10 cm^2 radiation field. The tuned initial energies of the monoenergetic beams are also given.

	Clinac			monoenergetic	
nominal energy	E_{ini}	Bremsstrahlung	R_{50}	R_{50}	E_{tuned}
[MeV]	[MeV]	[%]	[cm]	[cm]	[MeV]
6	7.27	0.7	2.54	2.53	6.47
9	10.21	1.1	3.73	3.73	9.22
12	13.37	2.6	4.98	4.98	12.11
15	16.61	3.4	6.27	6.27	15.15
16	17.80	4.2	6.70	6.72	16.19
18	19.97	5.1	7.50	7.51	18.12
20	22.23	6.3	8.24	8.25	19.96
22	24.46	6.5	9.01	9.03	21.96

or electron applicators. Using a database of modularized Varian linac components, penEasyLinac generates the material files, the configuration file (description of the initial beam parameters and tallies included in the simulation) and the geometry file (description of the linac by means of quadric surfaces using the syntax defined by pengeom, the geometry package distributed with penelope). The quality of the geometry files produced by penEasyLinac has been extensively tested by comparing the simulated dose profiles produced with these geometries with experimental data (Brualla *et al.* 2009, Sempau *et al.* 2011, Isambert *et al.* 2010, Brualla *et al.* 2012).

The simulations of these beams have been carried out in two steps. In the first one, phase-space files (PSFs) have been generated at a surface normal to the beam axis and immediately upstream the phantom entrance. These PSFs have been used in a second step as sources of particles to be transported through the water phantom.

Monoenergetic beams reproducing the R_{50} values of the eight aforementioned Clinac beams have been also considered. In order to tune these monoenergetic beams, the percentage depth dose curves for a 10×10 cm^2 radiation field (with a source-to-surface distance of 100 cm) have been estimated and compared to those produced by the PSFs of the linacs. Cylindrical scoring voxels of 0.5 cm of radial thickness and 0.2 cm of height, concentrical to the beam axis were used. Type A statistical uncertainties were maintained below 0.01 %. In the case of these monoenergetic beams, a mathematical collimation has been used to conform the radiation fields. This was done by discontinuing the transport of the particles arriving at the phantom entrance outside the defined square field.

Table 3.1 shows the values of R_{50} obtained for the different beams considered. The relative differences between the values corresponding to the full linac models and those found after tuning the monoenergetic beams are below 0.3 %. Just for comparison we can

say that these R_{50} differ from those quoted by Ding and Rogers (1995) for a Varian Clinac 2100 C by $0.20-0.27$ cm for all energies except for 6 MeV where the difference is 0.09 cm.

3.2.4. Simulation geometry

The simulation geometry was in accordance to the measuring conditions established in the TRS-398 protocol (IAEA 2000). A water phatom of $50 \times 50 \times 50$ cm^3 was situated at a source-to-surface distance of 100 cm. Results for irradiation fields of 10×10 cm^2 and 20×20 cm^2 were obtained. The reference point was at a depth $z_{\mathrm{ref}} = 0.6\, R_{50} - 0.1$ cm. The ionization chamber was situated in such a way that the surface separating the window (or the entrance widow) and the active collecting region was at z_{ref}. The absorbed dose scored within its active volume yields $D_{\mathrm{c,Q}}$. In these simulations standard type A uncertainties were below 0.4 % for the A10 chamber and 0.2 % for all the other chambers.

As reference we used a ^{60}Co gamma beam whose spectrum was taken from Mora and Maio (1999).

The scoring voxel considered to estimate the dose absorbed in water, $D_{\mathrm{w,Q}}$, was a cylinder with a radius of 1 cm and a height of 0.025 cm centered in the beam axis and situated at the reference depth. It is similar to that used by other authors in previous calculations (Zink and Wulff 2008, Zink and Wulff 2009, Zink and Wulff 2012, Muir and Rogers 2013).

3.3. Results

Figure 3.3 shows the $k_{\mathrm{Q,Q_0}}$ calculated for the seven ionization chambers studied and for radiation fields of 10×10 cm^2 (open squares) and 20×20 cm^2 (solid circles). Relative differences between both results are shown in the insets. The dotted curve for the P11 chamber was obtained from TG-51 (Almond *et al.* 1999) and TRS-398 (IAEA 2000) and is shown for comparison. As we can see, the result of our simulations for the lowest energy beam (6 MeV) is slightly larger than the $k_{\mathrm{Q,Q_0}}$ value of these protocols. For larger energies the TG-51/TRS-398 values agree reasonably well with those we have found.

The values of $k_{\mathrm{Q,Q_0}}$ found for 10×10 cm^2 are slightly above those obtained for 20×20 cm^2 and the effect becomes more evident for higher values of R_{50}. In the case of the A10 chamber, the maximum relative difference is ~ 0.8 % for $R_{50} \sim 3.7$ cm and the statistical uncertainties in the relative differences are 0.5-0.6 %. In all other cases, these uncertainties are around 0.3 % with a maximum relative difference of 0.6 % for the P11 chamber at $R_{50} \sim 7.5$ cm. The results obtained with the two field sizes are statistically compatible in all cases at 2σ level.

Figure 3.4 compares the results obtained with the PSFs for the detailed Clinac model beams (open squares) with those provided by the monoenergetic beams reproducing their R_{50} values (solid triangles). These results correspond to a 10×10 cm^2 radiation field

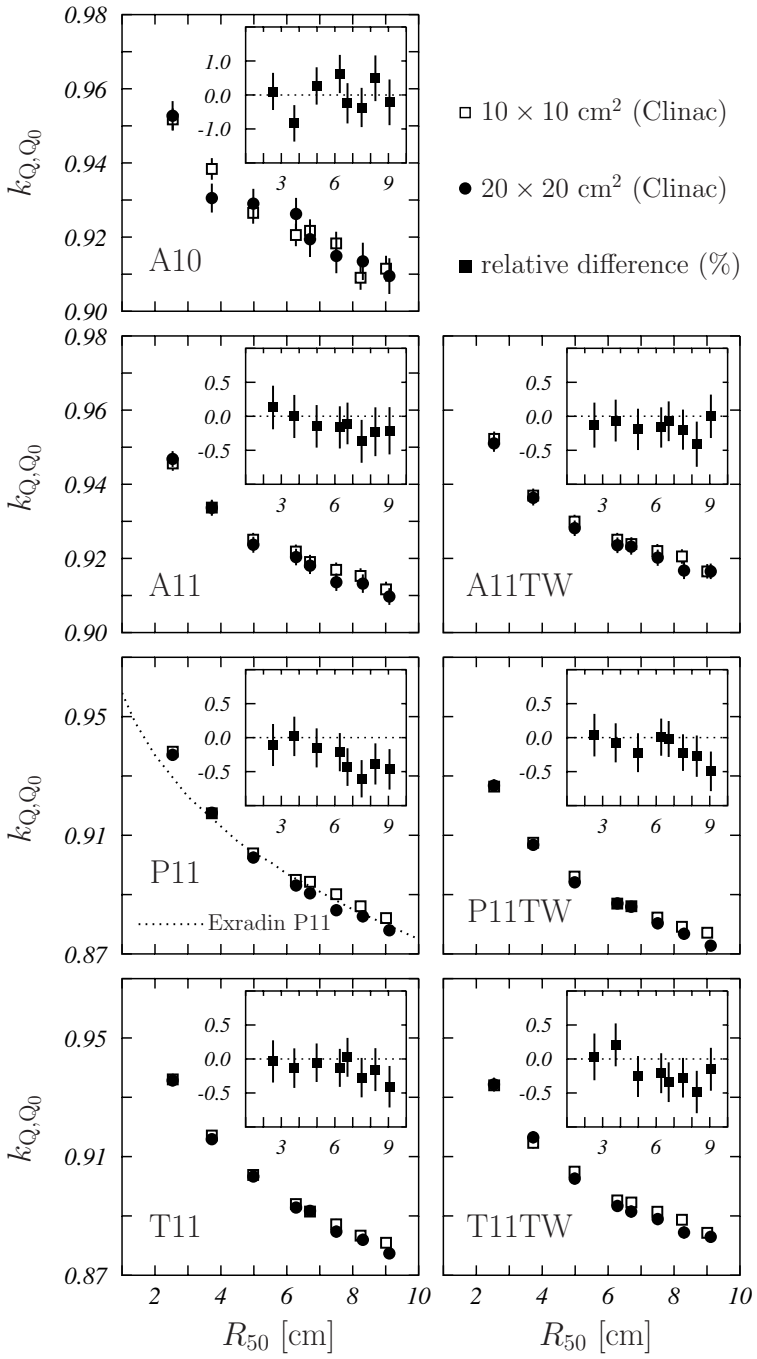

Figura 3.3: k_{Q,Q_0} calculated for the seven Exradin ionization chambers studied. Results obtained for the Clinac beams and for radiation fields of 10×10 *cm*^{2} *(open squares) and* 20×20 *cm*^{2} *(solid circles) are shown. The insets show the relative differences, in percentage, between the values obtained for both field sizes. Statistical uncertainties are given with a coverage factor* $k = 1$*. The dotted curve for the P11 chamber corresponds to the Exradin P11 chamber whose data have been taken from TG-51 (Almond et al. 1999) and TRS-398 (IAEA 2000) protocols. Numerical values of our results can be found in table 3.2.*

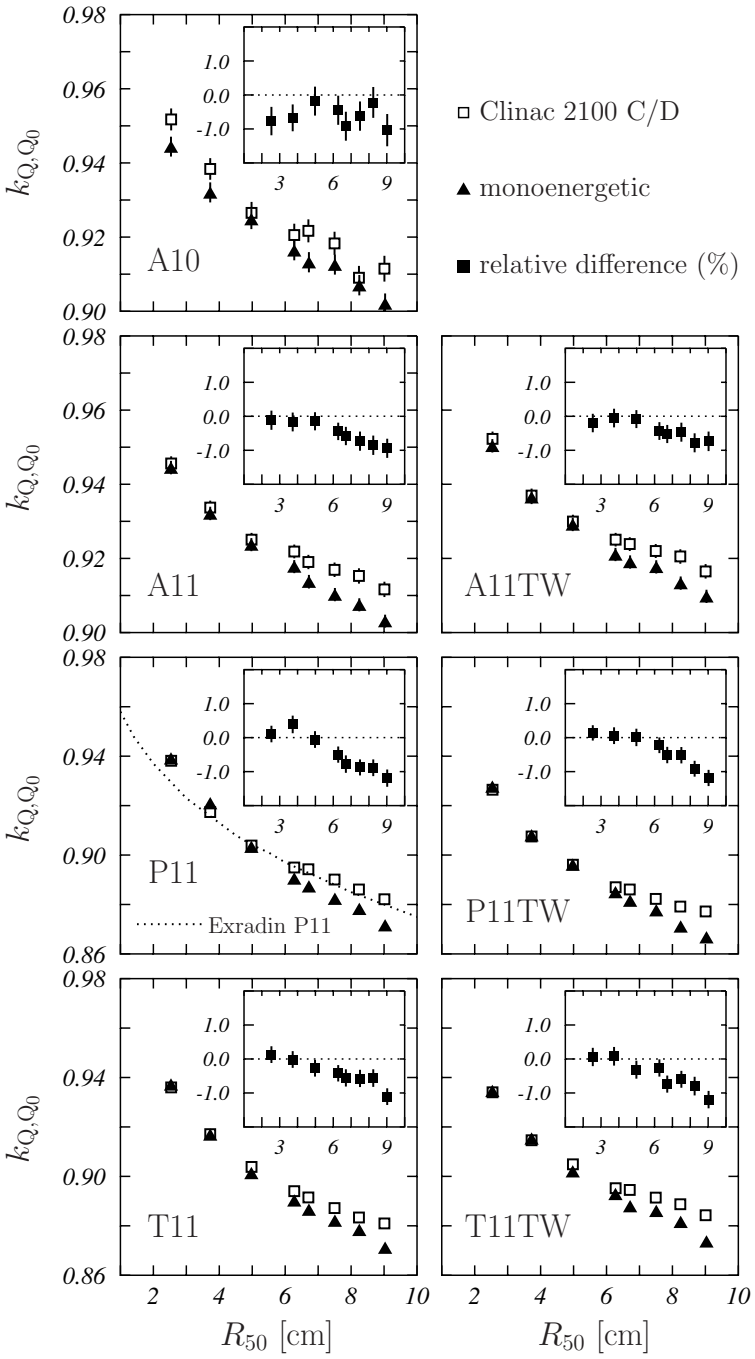

Figura 3.4: k_{Q,Q_0} calculated for the seven Exradin ionization chambers studied. Results obtained for the Clinac beams (open squares) are compared to those found with the monoenergetic beams reproducing their R_{50} values (solid triangles). Results shown are for a radiation field of 10×10 cm^2. The insets show the relative differences, in percentage, between the values obtained for both calculations. Statistical uncertainties are given with a coverage factor $k = 1$. The dotted curve for the P11 chamber corresponds to the Exradin P11 chamber whose data have been taken from TG-51 (Almond et al. 1999) and TRS-398 (IAEA 2000) protocols. Numerical values of our results can be found in table 3.2.

and the relative differences are shown in the insets. Again, the dotted curve for the P11 chamber corresponds to data from TG-51 (Almond *et al.* 1999) and TRS-398 (IAEA 2000). As it can be seen, they show a reasonable agreement with those we have found for the complete linac models.

The values obtained with the monoenergetic beams differ from those found for the detailed linac models for large energies and the discrepancies increase as R_{50} grows from ~ 6 cm until 9 cm reaching relative differences around 1 % in all cases. The largest one is 1.2 % and has been found for the T11TW chamber irradiated with the 22 MeV beam.

This was not the situation found by Sempau *et al.* (Sempau *et al.* 2004) who studied the beam quality correction factor for the Scanditronix NACP-02 and the Wellhöfer PPC-05 and PPC-40 ionization chambers. In that work a Siemens Mevatron KDS and a Varian Clinac 2300 C were considered and one of the main conclusions was that the results obtained with monoenergetic electron beams and with the complete linac geometries showed negligible differences for similar R_{50} values. This can be seen in the lower panel of figure 3.5 where the results of Sempau *et al.* are plotted with solid symbols.

To investigate this point we have repeated the calculations of Sempau *et al.* (2004) for the NACP-02 ionization chamber. To mimic as much as possible the simulations performed by these authors we have changed also the absorption energies to $E_{\mathrm{ABS}}(\mathrm{e}^-) = E_{\mathrm{ABS}}(\mathrm{e}^+) = 10^4$ eV and $E_{\mathrm{ABS}}(\gamma) = 10^3$ eV for all materials. The value of $f_{\mathrm{c,Q}}$ that we have obtained for ^{60}Co, using the spectrum of Mora and Maio (1999), was 1.1509 ± 0.0018 while that quoted by Panettieri *et al.* (2008) is 1.1575 ± 0.0012, the uncertainty being given in both cases with a coverage factor $k = 1$. The relative difference of 0.6 % between both results can be ascribed to differences in the geometries used, in the spectra of the ^{60}Co source and in the PENELOPE code version. In this respect it is worth mentioning that Muir *et al.* (2012) found that the changes in the details concerning the electrode at the rear of this chamber may account for up to 0.5 % differences in $f_{\mathrm{c,Q}}$ for ^{60}Co.

The results obtained with the complete linac model (open squares) and with the monoenergetic beam (open circles) are shown in figure 3.5, where they are compared to the values quoted in different previous works and to the values indicated in TG-51 (Almond *et al.* 1999) and TRS-398 (IAEA 2000) protocols (dotted curve). In the upper panel, the $k_{Q,Q_{\mathrm{in}}}$ values are compared to four sets of experimental data taken from McEwen and DuSautoy (2009) (solid symbols). The agreement between our results and the experimental ones is reasonably good. Also TG-51/TRS-398 values agree with our results. The fact that in this case the calibration quality is $\mathrm{Q_{in}} = 7.5\,\mathrm{g/cm^2}$ hides to a large extent the differences existing between the results that we have obtained with our PSF and monoenergetic calculations. However, these differences are apparent in the other two panels of figure 3.5 where $f_{\mathrm{c,Q}}$ values are shown. In the central panel our results are compared to those obtained by Buckley and Rogers (2006) (solid circles) and Araki (2008) (solid squares) in Monte Carlo simulations performed with the EGSnrc code for various linac models. The values quoted by these authors agree with those we have obtained with the complete linac models, while those we have found in the simulations with the monoenergetic beams are clearly below them. Our results agree very well with the data obtained from TG-51/TRS-398.

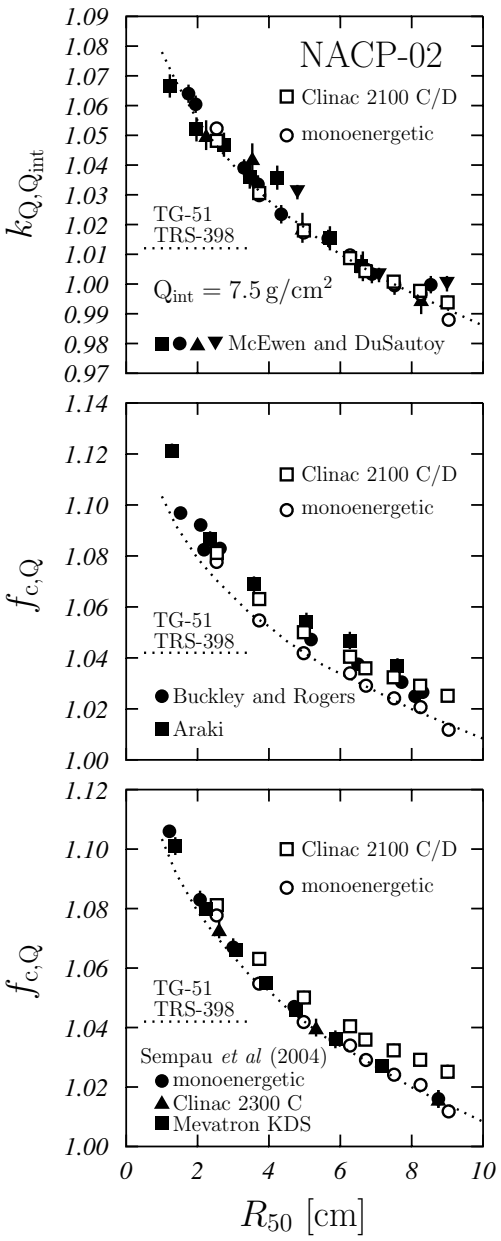

Figura 3.5: Comparison of the results obtained for the NACP-02 chamber with the Clinac (open squares) and the monoenergetic (open circles) beams with those quoted in previous works. Upper panel: $k_{Q,Q_{in}}$ (with $Q_{in} = 7.5\,g/cm^2$); four sets of experimental data from McEwen and DuSautoy (2009) are shown with solid symbols. Central panel: $f_{c,Q}$; EGSnrc Monte Carlo results from Buckley and Rogers (2006) and Araki (2008) for various linac models are shown with solid circles and squares, respectively. Lower panel: $f_{c,Q}$; values obtained by Sempau et al. (2004) for monoenergetic beams (solid circles) and for various beams of a Clinac 2300 C (solid triangles) and a Mevatron KDS (solid squares) linacs are shown. Dotted curve has been taken from TG-51 (Almond et al. 1999) and TRS-398 (IAEA 2000). Results shown are for a radiation field of 10×10 cm^2. Statistical uncertainties are given with a coverage factor $k = 1$. Numerical values of our results can be found in table 3.3.

In the lower panel, our $f_{c,Q}$ values are compared to the aforementioned results of Sempau *et al.* (2004). The results of these authors are in good agreement with those we have obtained in our calculations for the monoenergetic beams that, on the other hand, show differences with those found for the detailed linac models at high beam energies. These differences are similar to those observed for the Exradin ionization chambers. The maximum relative difference corresponds to the 22 MeV beam and is 0.87 %, which is of the same order (though slightly smaller) than the differences observed for the Exradin chambers.

It is not simple to identify the reasons of the differences observed. The calculations done by Sempau *et al.* (2004) for the detailed linac models were carried out with PSFs generated with a code developed by Sempau *et al.* (2001), in the case of the Siemens Mevatron KDS, and PSFs provided by Ma (as a private communication), in the case of the Varian Clinac 2300 C (that, *a priori*, shares the same geometry with the 2100 C/D model considered in our calculations). In this last case, the PSFs generated by Ma at that time may had been subjected to the geometry deficiencies that Chibani and Ma (2007) pointed out later. One of the main points in this respect was the absence of the secondary collimator (lead shield). In order to understand the effect that this collimator could produce, we have performed a new set of calculations with PSFs generated with the complete geometry of the linac head by eliminating the secondary collimator in our geometry. The results obtained have not shown statistically significant differences with those found for the complete linac head. This is due to the fact that in the case of electron beams the electron applicator, which is present to guarantee the radiation field size, is the main responsible for the beam definition at the phantom entrance.

Finally, we have performed an additional calculation considering the complete Clinac geometry but stopping all photons generated in the head and the air path to the phantom

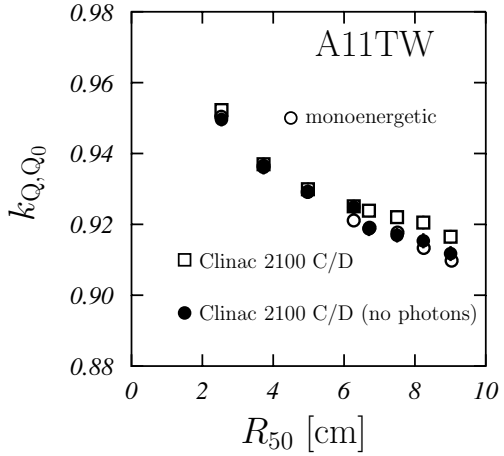

Figura 3.6: k_{Q,Q_0} calculated for the A11TW ionization chamber. Results obtained for the Clinac beams (open squares) are compared to those found stopping all photons at the water phantom entrance (solid circles). Also the values found for the monoenergetic beams reproducing the corresponding R_{50} values (open circles). Results shown are for a radiation field of 10×10 cm^2. Statistical uncertainties are given with a coverage factor $k = 1$ and in most cases are smaller than the size of the symbols used.

at its entrance. The results obtained in this "incomplete" simulation are shown for the A11TW ionization chamber in figure 3.6 (solid circles). It is observed how these results are close to those found for the mononergetic beams (open circles) and differ significantly at large energies from those found with the complete linac geometries (open squares). This indicates that a large part of the differences observed between the k_{Q,Q_0} obtained for the detailed linac models and for the monoenergetic beams are due to the presence of the photons produced as secondary particles in the various elements of the linac geometry as well as in the air path between the linac head and the phantom surface. This is not surprising because, as quoted in table 3.1 the contribution of the Bremsstrahlung tail is not negligible and grows with the energy of the beam. Muir and Rogers (2013) found a similar effect in the PTW Roos ionization chamber for $R_{50} \leq 7\,\text{cm}$. The reason for this behavior may be linked to the increase of the stopping-power ratios (up to $\sim 0.5\,\%$, depending on the particular linac considered) due to contaminant photons (Ding *et al.* 1995). It is worth mentioning that these results disagree with the findings of Sempau *et al.* (2004) who stated that for the Siemens Mevatron at 18 MeV there was no difference between the $k_{Q,Q_{\text{int}}}$ calculated with and without considering the photons present in the PSF.

The fact that some of the chambers studied share the same geometry, with changes in the material conforming some of their constituent elements, has permitted us to study the effect that these material changes produce in the quality correction factor. In figure 3.7 we show the ratios of k_{Q,Q_0} values obtained for couples of chambers, specifically "A" and "P" (upper panel), "A" and "T" (central panel) and "P" and "T" (lower panel). Circles correspond to the "TW" chamber type and squares to the other ones. Finally, open symbols show the results obtained for the various Clinac qualities whereas solid symbols correspond to the monoenergetic beams.

A first point to note is the overall agreement between the results obtained with the Clinac PSFs and the monoenergetic beams. The discrepancies observed at the larger energies in figure 3.4 disappear, showing that the effect of the change of material is the same independently of the radiation source considered.

The new materials used in the "P" and "T" chambers instead of the C552 (used in the "A" chambers), D400 and A150, respectively, have similar densities (1.16 g/cm^3 and 1.13 g/cm^3). However, the material change does not affect in the same way the response of the "P" and "T" chambers as it can be seen in the two upper panels of figure 3.7. The corresponding differences are summarized in the lower panel of this figure. Therein it is seen that the ratio of the k_{Q,Q_0} values obtained for the P11TW and T11TW chambers remains almost constant and close to 1 for all beam qualities considered. The ratio for the P11 and T11 chambers is also approximately constant but $\sim 1\,\%$ smaller. Looking at the chamber geometries in figure 3.1, we see that the main difference between A11 (P11 and T11) chambers and the "TW" partners is the presence of the thin-window support rings that produces a notable modification of the geometry structure. There is also a difference in the active volume of the chambers (see Sect. 3.2.1). Finally, though the densities are similar, the material compositions are different: D100 is CH, A150 has, apart from C and H, a non-negligible quantity of both N and O and a small quantity of F and Ca, and C552 is basically H, C and F in similar quantity plus small parts of O and Si. The combined

effect of these differences does not factorize in the calculated ratios and the difference commented appears.

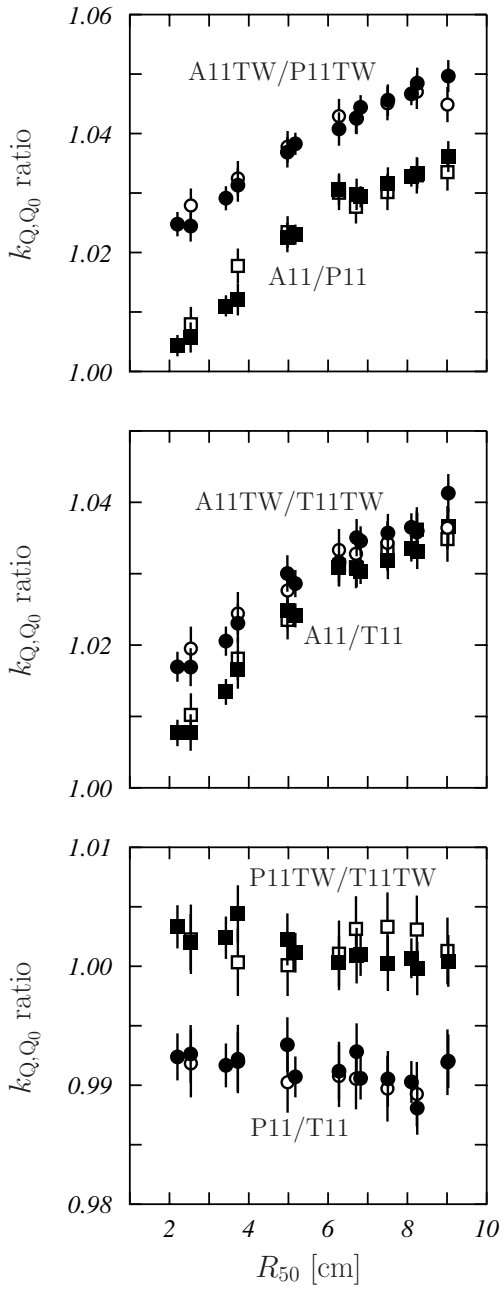

Figura 3.7: Ratios of k_{Q,Q_0} values for ionization chamber couples: A and P (upper panel), A and T (medium panel) and P and T (lower panel). Circles correspond to TW chambers and squares to other model. Open symbols show the results obtained for the Clinac beams and solid symbols to the monoenergetic ones. Statistical uncertainties are given with a coverage factor $k = 1$.

3.4. Conclusions

In this work, the Monte Carlo code PENELOPE/PENEASY was used to calculate the beam quality correction factor, k_{Q,Q_0} for seven Exradin ionization chambers. Electron beams, with nominal electron energies ranging between 6 and 22 MeV, were simulated for a Varian Clinac 2100 C/D using geometries generated with the PENEASYLINAC code. Those simulations tallied PSFs at the phantom surface. In a second step of the calculation, these PSFs were transported through the phantom to calculate the absorbed dose in water and in the air cavity of the real detector that permitted to determine the overall perturbation factor $f_{c,Q}$ and the corresponding k_{Q,Q_0}. These factors were also calculated for monoenergetic beams that reproduced the R_{50} quality index of the Varian beams.

No differences in the correction factor were found when a different radiation field size is considered. In fact, the results obtained for a 10×10 cm^2 and a 20×20 cm^2 were statistically compatible.

For the lower energy beams, below 12 MeV, the values of k_{Q,Q_0} determined for both the Clinac and the monoenergetic beams were in agreement, as quoted in previous works. However, with increasing energies, the values found for the electron beams produced from linacs were $\sim 1\,\%$ above those obtained with the monoenergetic beams, something that was not observed in a previous work in which the agreement between both types of calculations was excellent. It has been proved that a major part of this discrepancy can be ascribed to the secondary photons produced in the geometry elements of the linacs as well as in the air path between the linac head and the phantom.

The use of the D400 and A150 plastics instead of the C552 in some of the chambers analyzed gives rise to modifications of the quality correction factor that depend on the specific geometry of the chamber.

Acknowledgements

This work has been supported in part by the Junta de Andalucía (FQM0220) and by the Ministerio de Economía y Competitividad (FPA2012-31993 and FIS2012-38480) and the European Regional Development Fund (ERDF). LB acknowledges financial support from the Deutsche Forschungsgemeinschaft project BR 4043/1-1.

Appendix

In this appendix we summarize the values of the k_{Q,Q_0} factors obtained in our simulations and corresponding to the Standard Imaging Exradin ionization chambers, as well as those of the NACP-02 chamber.

Tabla 3.2: k_{Q,Q_0} values obtained in our simulations for the seven Exradin ionization chambers. The results found for the Clinac (with $10 \times 10\,cm^2$ and $20 \times 20\,cm^2$ fields) and monoenergetic (with a field of $10 \times 10\,cm^2$) beams are shown. The uncertainty (with a coverage factor $k = 1$) is given between parentheses; thus, 0.925(3) meand 0.925 ± 0.003.

	k_{Q,Q_0}				
	Clinac			monoenergetic	
chamber	R_{50} [cm]	$10 \times 10\,cm^2$	$20 \times 20\,cm^2$	R_{50} [cm]	$10 \times 10\,cm^2$
A10	2.54	0.952(3)	0.953(4)	2.53	0.944(3)
	3.73	0.938(3)	0.931(4)	3.73	0.932(3)
	4.98	0.927(3)	0.929(4)	4.98	0.925(3)
	6.27	0.921(3)	0.926(4)	6.27	0.916(3)
	6.70	0.922(3)	0.919(5)	6.72	0.913(3)
	7.50	0.918(3)	0.915(5)	7.51	0.913(3)
	8.24	0.909(3)	0.913(5)	8.25	0.907(3)
	9.01	0.911(3)	0.909(5)	9.03	0.902(3)
A11	2.54	0.946(2)	0.947(2)	2.53	0.944(2)
	3.73	0.934(2)	0.934(2)	3.73	0.932(2)
	4.98	0.925(2)	0.924(2)	4.98	0.924(2)
	6.27	0.922(2)	0.920(2)	6.27	0.918(2)
	6.70	0.919(2)	0.918(2)	6.72	0.914(2)
	7.50	0.917(2)	0.914(2)	7.51	0.910(2)
	8.24	0.915(2)	0.913(2)	8.25	0.907(2)
	9.01	0.912(2)	0.910(2)	9.03	0.903(2)
A11TW	2.54	0.952(2)	0.951(2)	2.53	0.950(2)
	3.73	0.937(2)	0.936(2)	3.73	0.936(2)
	4.98	0.930(2)	0.928(2)	4.98	0.929(2)
	6.27	0.925(2)	0.924(2)	6.27	0.921(2)
	6.70	0.924(2)	0.923(2)	6.72	0.919(2)
	7.50	0.922(2)	0.920(2)	7.51	0.918(2)
	8.24	0.921(2)	0.917(2)	8.25	0.913(2)
	9.01	0.917(2)	0.916(2)	9.03	0.910(2)
P11	2.54	0.938(2)	0.937(2)	2.53	0.939(2)
	3.73	0.917(2)	0.918(2)	3.73	0.921(2)
	4.98	0.904(2)	0.903(2)	4.98	0.903(1)
	6.27	0.895(2)	0.893(2)	6.27	0.890(1)
	6.70	0.894(2)	0.890(2)	6.72	0.887(2)
	7.50	0.890(2)	0.885(2)	7.51	0.882(1)
	8.24	0.886(2)	0.883(2)	8.25	0.878(1)
	9.01	0.882(2)	0.878(2)	9.03	0.872(1)
P11TW	2.54	0.926(2)	0.927(2)	2.53	0.928(2)
	3.73	0.907(2)	0.907(2)	3.73	0.908(2)
	4.98	0.896(2)	0.894(2)	4.98	0.896(2)
	6.27	0.887(2)	0.887(2)	6.27	0.885(2)
	6.70	0.886(2)	0.886(2)	6.72	0.882(2)
	7.50	0.882(2)	0.880(2)	7.51	0.878(1)
	8.24	0.879(2)	0.877(2)	8.25	0.871(1)
	9.01	0.877(2)	0.873(2)	9.03	0.867(1)
T11	2.54	0.936(2)	0.936(2)	2.53	0.937(2)
	3.73	0.917(2)	0.916(2)	3.73	0.917(1)
	4.98	0.904(2)	0.903(2)	4.98	0.901(1)
	6.27	0.894(2)	0.893(2)	6.27	0.890(1)
	6.70	0.891(2)	0.892(2)	6.72	0.887(1)
	7.50	0.887(2)	0.885(2)	7.51	0.882(1)
	8.24	0.883(2)	0.882(2)	8.25	0.878(1)
	9.01	0.881(2)	0.877(2)	9.03	0.871(1)
T11TW	2.54	0.934(2)	0.934(2)	2.53	0.935(2)
	3.73	0.915(2)	0.917(2)	3.73	0.915(2)
	4.98	0.905(2)	0.903(2)	4.98	0.902(2)
	6.27	0.895(2)	0.893(2)	6.27	0.893(2)
	6.70	0.895(2)	0.891(2)	6.72	0.888(2)
	7.50	0.891(2)	0.889(2)	7.51	0.886(2)
	8.24	0.889(2)	0.884(2)	8.25	0.882(1)
	9.01	0.884(2)	0.883(2)	9.03	0.874(1)

Tabla 3.3: $k_{Q,Q_{int}}$ *(*$Q_{int} = 7.5\,g/cm^2$*) and* $f_{c,Q}$ *values obtained in our simulations for the NACP-02 ionization chamber. The results found for the Clinac and monoenergetic beams, with a field of* $10 \times 10\,cm^2$*, are shown. The uncertainty (with a coverage factor* $k = 1$*) is given between parentheses; thus, 1.031(2) meand* 1.031 ± 0.002*.*

	NACP-02			
	Clinac		monoenergetic	
chamber	R_{50} [cm]	$10 \times 10\,cm^2$	R_{50} [cm]	$10 \times 10\,cm^2$
$k_{Q,Q_{int}}$	2.54	1.048(2)	2.53	1.052(1)
	3.73	1.031(2)	3.73	1.030(1)
	4.98	1.018(2)	4.98	1.017(1)
	6.27	1.009(2)	6.27	1.010(1)
	6.70	1.004(2)	6.72	1.005(1)
	7.45	1.001(2)	7.51	1.000(1)
	8.24	0.998(2)	8.25	0.997(1)
	9.01	0.994(2)	9.03	0.988(1)
$f_{c,Q}$	2.54	1.081(2)	2.53	1.078(1)
	3.73	1.063(2)	3.73	1.055(1)
	4.98	1.050(2)	4.98	1.042(1)
	6.27	1.040(2)	6.27	1.034(1)
	6.70	1.036(2)	6.72	1.029(1)
	7.50	1.032(2)	7.51	1.024(1)
	8.24	1.029(2)	8.25	1.021(1)
	9.01	1.025(2)	9.03	1.012(1)

Almond P R, Biggs P J , Coursey B M, Hanson W F, Saiful Huq M, Nath R and Rogers D W O 1999 AAPM's TG-51 protocol for clinical reference dosimetry of high-energy photon and electron beams *Med. Phys.* **26**, 1847-70

Araki F 2008 Monte Carlo calculations of correction factors for plane-parallel ionization chambers in clinical electron dosimetry *Med. Phys.* **35**, 4033-40

Brualla L, Palanco-Zamora R, Wittig A, Sempau J and Sauerwein W 2009 Comparison between PENELOPE and electron Monte Carlo simulations of electron fields used in the treatment of conjunctival lymphoma *Phys. Med. Biol.* **54** 5469-81

Brualla L, Zaragoza F J, Sempau J, Wittig A and Sauerwein W 2012 Electron irradiation of conjunctival lymphoma–Monte Carlo simulation of the minute dose distribution and technique optimization *Int. J. Radiat. Oncol. Biol. Phys.* **83** 1330-7

Buckley L A and Rogers D W O 2006 Wall correction factors, P_{wall}, for parallel-plate ionization chambers *Med. Phys.* **33** 1788-96

Capote R, Sánchez-Doblado F, Leal A, Lagares J I, Arráns R and Hartmann G H 2004 An EGSnrc Monte Carlo study of the microionization chamber for reference dosimetry of narrow irregular IMRT beamlets *Med. Phys.* **31** 2416-22

Chibani O and Ma C-M 2007 On the discrepancies between Monte Carlo dose calculations and measurements for the 18 MV Varian photon beam *Med. Phys.* **34** 1206-16

Ding G X and Rogers D W O 1995 Energy spectra, angular spread, and dose distributions of electron beams from various accelerators used in radiotherapy, NRC Report PIRS 0439 (Ottawa:NRC)

Ding G X, Rogers D W O and Mackie T R 1995 Calculation of stopping-power ratios using realistic clinical electron beams *Med. Phys.* **22** 489-501

Erazo F and Lallena A M 2013 Calculation of beam quality correction factors for various thimble ionization chambers using the Monte Carlo code PENELOPE *Physica Medica: Eur. J. Med. Phys.* **29**, 163-70

Faddegon B A, Asai M, Perl J, Ross C, Sempau J, Tinslay J and Salvat F 2008 Benchmarking of Monte Carlo simulation of bremsstrahlung from thick targets at radiotherapy energies *Med. Phys.* **35** 4308-17

Faddegon B A, Kawrakow I, Kubyshin Y, Perl J, Sempau J and Urban L 2009 The accuracy of EGSnrc, Geant4 and PENELOPE Monte Carlo systems for the simulation of electron scatter in external beam radiotherapy *Phys. Med. Biol.* **54** 6151-63

Fernández-Varea J M, Carrasco P, Panettieri V and Brualla L 2007 Monte Carlo based water/medium stopping-power ratios for various ICRP and ICRU tissues *Phys. Med. Biol.* **52** 6475-83

González-Castaño D M, Hartmann G H, Sánchez-Doblado F, Gómez F, Kapsch R-P, Pena J and Capote R 2009 The determination of beam quality correction factors: Monte Carlo simulations and measurements *Phys. Med. Biol.* **54**, 4723-41

International Atomic Energy Agency 2000 Absorbed dose determination in external beam radiotherapy: an International Code of Practice for dosimetry based on standards of absorbed dose to water IAEA Technical Report Series 398 (Vienna:IAEA)

Isambert A, Brualla L, Benkebil M and Lefkopoulos D 2010 Determination of the optimal statistical uncertainty to perform electron-beam Monte Carlo absorbed dose estimation in the target volume *Cancer Radiother.* **14** 89-95

Jang S Y, Liu H H, Mohan R and Siebers J V 2007 Variations in energy spectra and water-to-material stopping-power ratios in three-dimensional conformal and intensity-modulated photon fields *Med. Phys.* **34** 1388-97

McEwen M R and DuSautoy A R 2009 Primary standards of absorbed dose for electron beams *Metrologia* **46** S59-S79

Mora G M and Maio A 1999 Monte Carlo simulation of a typical Co^{60} therapy source *Med. Phys.* **26** 1847-70

Muir B R and Rogers D W O 2010 Monte Carlo calculations of k_Q, the beam quality conversion factor *Med. Phys.* **37** 5939-50

Muir B R, McEwen M R and Rogers D W O 2012 Beam quality conversion factors for parallel-plate ionization chambers in MV photon beams *Med. Phys.* **39**, 1618-31

Muir B R and Rogers D W O 2013 Monte Carlo calculations for reference dosimetry of electron beams with the PTW Roos and NE2571 ion chambers *Med. Phys.* **40** 121722

Nahum A E 1978 Water/air mass stopping power ratios for megavoltage photon and electron beams *Phys. Med. Biol.* **23** 24-38

Panettieri V, Sempau J and Andreo P 2008 Chamber-quality factors in Co-60 for three plane-parallel chambers for the dosimetry of electrons, protons and heavy charged particles: PENELOPE Monte Carlo simulations *Phys. Med. Biol.* **53** 5917-26

Salvat F and Fernández-Varea J M 2009 Overview of physical interaction models for photon and electron transport used in Monte Carlo codes *Metrologia* **46** S112-38

Salvat F, Fernández-Varea J M and Sempau J 2011 PENELOPE - A Code System for Monte Carlo simulation of electron and photon transport (Issy-les-Moulineaux:OECD Nuclear Energy Agency)

Sempau J, Sánchez-Reyes A, Salvat F, Oulad Ben Tahar H, Jiang S B and Fernández-Varea J M 2001 Monte Carlo simulation of electron beams from an accelerator head using PENELOPE *Phys. Med. Biol.* **46** 1163-86

Sempau J, Fernández-Varea J M, Acosta E and Salvat F 2003 Experimental benchmarks of the Monte Carlo code PENELOPE *Nucl. Instrum. Meth. Phys. Res. B* **207** 107-23

Sempau J, Andreo P, Aldana J, Mazurier J and Salvat F 2004 Electron beam quality correction factors for plane-parallel ionization chambers: Monte Carlo calculations using the PENELOPE system *Phys. Med. Biol.* **49** 4427-44

Sempau J and Andreo P 2006 Configuration of the electron transport algorithm of PENELOPE to simulate ion chambers *Phys. Med. Biol.* **51** 3533-48

Sempau J 2009 PENEASY: A modular main program and voxelized geometry package for PENELOPE Available at www.upc.edu/inte/downloads/penEasy.htm (accessed 23rd May 2014).

Sempau J, Badal A and Brualla L 2011 A PENELOPE-based system for the automated Monte Carlo simulation of clinacs and voxelized geometries–application to far-from-axis fields *Med. Phys.* **38** 5887-95

Siebers J V, Keall P J, Nahum A E and Mohan R 2000 Converting absorbed dose to medium to absorbed dose to water for Monte Carlo based photon beam dose calculations *Phys. Med. Biol.* **45** 983-95

Svensson H and Brahme A 1986 Recent advances in electron and photon dosimetry, in *Radiation Dosimetry*, edited by C. G. Orton (New York:Plenum)

Vilches M, García-Pareja S, Guerrero R, Anguiano M and Lallena A M 2009 Multiple scattering of 13 and 20 MeV electrons by thin foils: A Monte Carlo study with GEANT, Geant4 and PENELOPE *Med. Phys.* **36** 3964-70

Williams A J, McEwen M R and DuSautoy A R 1998 A calculation of the water to graphite perturbation factor ratios for the NACP type 02 ionisation chamber using Monte Carlo techniques, NPL Report CIRM 13 (Teddington:National Physical Laboratory)

Yi C, Hah S and Yeom M S 2006 Monte Carlo calculation of the ionization chamber response to ^{60}Co beam using PENELOPE *Med. Phys.* **33**, 1213-21

Zink K and Wulff J 2008 Monte Carlo calculations of beam quality correction factors k_{Q} for electron dosimetry with a parallel-plate Roos chamber *Phys. Med. Biol.* **53** 1595-607

Zink K and Wulff J 2009 Positioning of a plane-parallel ionization chamber in clinical electron beams and the impact on perturbation factors *Phys. Med. Biol.* **54** 2421-35

Zink K and Wulff J 2012 Beam quality corrections for parallel-plate ion chambers in electron reference dosimetry *Phys. Med. Biol.* **57** 1831-54

Capítulo 4

Nuevas cámaras de dedal

Physica Medica: European Journal of Medical Physics (2015) [en prensa]

Photon beam quality correction factors for the NE2571A and NE2581A thimble ionization chambers using PENELOPE

Fabián Erazo[1,2] and Antonio M Lallena[1]

[1] Departamento de Física Atómica, Molecular y Nuclear, Universidad de Granada, E-18071 Granada, Spain
[2] Instituto del Cáncer - SOLCA, Cuenca, Ecuador

The beam quality correction factor k_{Q,Q_0} and the perturbation factor p_Q for photon beams were calculated for the NE2571A and NE2581A ionization chambers, using the Monte Carlo simulation code PENELOPE. Results are compared to those quoted for the NE2571 and NE2581 chambers in previous works. Both k_{Q,Q_0} and p_Q obtained for NE2571A and NE2581A chambers agree with those of their predecessors NE2571 and NE2581 ones.

4.1. Introduction

According to the codes of practice for dosimetry in radiotherapy (see e.g., TG51 [1] and TRS-398 [2]), the dose to water in a given point and for a given photon beam quality Q, $D_{\mathrm{w,Q}}$, is related to the dose measured by an ionization chamber situated at the same point, $D_{\mathrm{c,Q}}$, as:

$$D_{\mathrm{w,Q}} \,=\, D_{\mathrm{c,Q}} \cdot (s_{\mathrm{w,air}})_{\mathrm{Q}} \cdot p_{\mathrm{Q}}\,, \tag{4.1}$$

where $(s_{\mathrm{w,air}})_{\mathrm{Q}}$ is the stopping-power ratio between water and air and p_{Q} is an overall perturbation factor that takes into account all the effects due to the fact that the materials of the ionization chamber are not equivalent to the water conforming the medium where measurements are performed.

In practice, it is also of interest the factor [2]

$$k_{\mathrm{Q,Q_0}} \,=\, \frac{p_{\mathrm{Q}}}{p_{\mathrm{Q_0}}}\,\frac{(s_{\mathrm{w,air}})_{\mathrm{Q}}}{(s_{\mathrm{w,air}})_{\mathrm{Q_0}}} \,=\, \left(\frac{D_{\mathrm{w,Q}}}{D_{\mathrm{c,Q}}}\right)\cdot\left(\frac{D_{\mathrm{w,Q_0}}}{D_{\mathrm{c,Q_0}}}\right)^{-1}\,, \tag{4.2}$$

which is usually known as the beam quality correction factor and accounts for the differences between the beam quality Q available to the final user and the quality $\mathrm{Q_0}$ (usually that of a ^{60}Co gamma beam) at which the reference laboratory calibrates the ionization chamber. The measurement of either p_{Q} or $k_{\mathrm{Q,Q_0}}$ is difficult and in TRS-398 [2] values of $k_{\mathrm{Q,Q_0}}$ where adapted from calculations by Andreo [3]. More recently, other authors [4,5] have proposed to calculate the beam quality correction factor via Monte Carlo simulation, using the ratio

$$k_{\mathrm{Q,Q_0}} \,=\, \frac{f_{\mathrm{c,Q}}}{f_{\mathrm{c,Q_0}}}\,. \tag{4.3}$$

Here $f_{\mathrm{c,Q}}$ indicates an overall factor that depends on both the particular ionization chamber used and the beam quality, and relates directly the absorbed dose in the water with the absorbed dose in the chamber according to

$$D_{\mathrm{w,Q}} \,=\, D_{\mathrm{c,Q}} \cdot f_{\mathrm{c,Q}}\,. \tag{4.4}$$

By comparing this expression with equation (4.1), one may consider $f_{\mathrm{c,Q}}$ as an effective stopping-power ratio which is calculated taking into account, in the appropriate way, all the effects due to the actual presence of the chamber inside the water. The Monte Carlo procedure follows by obtaining both $D_{\mathrm{w,Q}}$ and $D_{\mathrm{c,Q}}$ for various beam qualities, including Q_0, and calculating $k_{\mathrm{Q,Q_0}}$ using equations (4.3) and (4.4). Of course this computational approach will be trustworthy only if the accurate geometries of the ionization chambers are available.

In this work we have analyzed the NE2571A and NE2581A Farmer-type chambers, manufactured by QADOS (Sandhurst, UK). To the best of our knowledge, no information about the beam quality correction factors and overall perturbation factors of these chambers has been previously published. The results obtained have been compared to those found for the predecessor NE2571 and NE2581 chambers in [6,7]. All simulations have been performed with the Monte Carlo code PENELOPE [8].

4.2. Material and methods

NE2571A and NE2581A thimble ionization chambers are Farmer-type chambers with sensitive volumes of 0.69 and 0.56 cm^3, respectively. Figure 4.1 shows a schematic drawing of the geometries of both chambers used in our simulations and extracted from the information provided by the manufacturer (QADOS). They have an external diameter of 0.86 cm and a length (including the connecting cable) of 9 cm, approximately. The air cavity of the two chambers has a diameter of 0.63 cm and a length of 2.41 cm. In the NE2571A chamber, the thimble is made of graphite, with a wall thickness of 0.036 cm, and the inner electrode of Al, with 0.1 cm of diameter. In the NE2581A chamber, the thimble (with a width of 0.036 cm) and the electrode (with a diameter of 0.3 cm) are both made of Shonka A-150. The insulator between the electrode and the wall is made of PTFE (polytetrafluoroethylene) in both chambers.

The corresponding correction factors were calculated with the Monte Carlo code PENELOPE (v. 2011) [8], a code that has been benchmarked in very different situations of interest in medical physics involving a wide range of energies [9–14]. The simulation procedure followed here was the same as the one used in [7] for the NE2571 ionization chamber. Simulations were carried out with the code penEasy [15], a steering code to run PENELOPE, adapted within clonEasy [16], a procedure that permits parallel simulation. The evaluation of Monte Carlo estimates and the corresponding statistical uncertainties was done according to [4,8].

PENELOPE transports photons in a detailed way and electrons and positrons in a mixed scheme [8]. The tracking parameters used in the code are C_1, C_2, W_{cc} and W_{cr} that affect the electron/positron transport. In addition, one must choose the parameter s_{max}, which fixes the maximum step length between particle interactions. All these parameters must be established for each material in the geometry. Absorption energies must be also

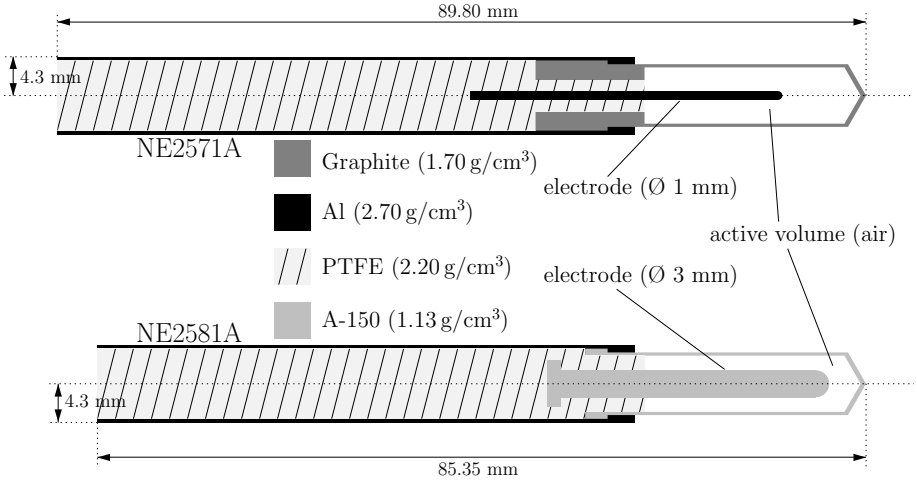

Figura 4.1: Scheme of the geometry of the NE2571A and NE2581A ionization chambers used in our simulations.

fixed; they determine the end of the track simulation and must be chosen for each particle type and each material.

In our simulations we used the same values for the transport parameters as those considered in reference [7] because we compared the results of the present simulations for the new chamber NE2571A to those we found for the NE2571 in that work. Specifically we took $C_1 = C_2 = 0.02$ for all the materials forming the ionization chambers (graphite, Al and PTFE, for the NE2571A; Al, PTFE and A-150, for the NE2581A, and the respective air-cavities) and for the water volume that surrounds it, up to 2 cm. The remaining water of the phantom and the air volume involving the whole geometry were simulated with $C_1 = C_2 = 0.1$. The threshold parameters were $W_{\rm cc} = 0.01 \cdot E_{\rm max}$ and $W_{\rm cr} = 0.001 \cdot E_{\rm max}$, $E_{\rm max}$ being the maximum energy of the initial particles. The absorption energies were chosen to be $E_{\rm abs}(e^-, e^+) = W_{\rm cc}$ and $E_{\rm abs}(\gamma) = W_{cr}$. Reducing these values does not change the results of the simulations while increases the CPU calculation time. Finally, for $s_{\rm max}$ we used one tenth of the thickness of each material in the geometry, as it is suggested in the code manual [8].

The radiation sources considered in this work were the same as those used in [7]: a ^{60}Co gamma beam with the spectrum quoted in [17] (that we considered as our reference quality Q_0) and photon beams generated by different linear accelerators (a Varian Clinac LE of 4 MV, a Varian Clinac HE of 6, 10, 15 and 18 MV, a Siemens KD of 6 and 18 MV and an Elekta SL25 of 6 and 25 MV) with the spectra calculated in [18].

Simulations were done using the geometrical source-to-surface setup proposed in TRS-398 [2]. We assumed point sources emitting photons with the corresponding spectra, whereas the ionization chamber was situated in the beam axis, inside a water phantom of $50 \times 50 \times 50\,\mathrm{cm}^3$, at the reference depth (5 cm for ^{60}Co and 10 cm for the MV photon sources). A source-to-surface distance of 100 cm and a radiation field of $10 \times 10\,\mathrm{cm}^2$ at the surface of the phantom were chosen. With this setup $D_{\rm c,Q}$ was calculated as the dose in the active volume of the chamber. On the other hand, $D_{\rm w,Q}$ was estimated, following reference [19], as the dose in a cylinder with a radius of 1 cm and a height of 0.025 cm situated at the reference point. In both cases, the energy lost by the transported particles in the corresponding regions of interest was scored and, once the simulation was completed, the doses were calculated by dividing the total accumulated energies by the masses of the respective scoring regions.

$\mathrm{TPR}^{20}_{10}(\mathrm{Q})$ values were calculated for the various beam qualities in separate Monte Carlo simulations as the ratios of the dose absorbed in water at depths of 20 and 10 cm, with a distance between the source and the measurement depths of 100 cm and a field at these depths of $10 \times 10\,\mathrm{cm}^2$. Depending on the energy and the specific linac considered, the total number of initial particles simulated ranged between 2 and $5 \cdot 10^9$. The statistical uncertainties of the depth doses in the water phantom calculated in the simulations were below 0.01 % (with a coverage factor $k = 2$).

The factors $f_{\rm c,Q}$ were calculated using equation (4.4) for the various beam qualities and, using them, the $k_{\mathrm{Q,Q_0}}$ values were determined with equation (4.3). A sigmoid function of $x \equiv \mathrm{TPR}^{20}_{10}(\mathrm{Q})$,

$$f(x) \;=\; s\left(1 - \exp\left[\frac{x \,-\, t}{u}\right]\right)\,, \tag{4.5}$$

was fitted to the results obtained for $k_{\mathrm{Q,Q_0}}$. Here s was chosen to be

$$s \;=\; \left(1 - \exp\left[\frac{x_0 \;-\; t}{u}\right]\right)^{-1} \tag{4.6}$$

where $x_0 \equiv \mathrm{TPR}^{20}_{10}(\mathrm{Q_0})$; this guaranteed that $f(x_0) = 1$.

Systematic uncertainties were also considered. We followed the analysis of Muir and Rogers [6] and Wulff *et al.* [20]. Muir and Rogers investigated the sources of type B uncertainties in different ionization chambers and found that the largest ones occurred due to (i) the assumption of a constant average energy lost per charge unit released by electrons in air and (ii) the uncertainty in the cross-section for photons in water. They quoted maximum relative uncertainties of 0.43 % for the NE2571 chamber, but they did not study the variation with the beam quality. On the other hand, Wulff *et al.* indicated that systematic uncertainties were mainly due to the electron cross sections involved in the calculations and for the NE2571 chamber they found 0.2 %, for 6MV sources, up to 0.4 %, for 24 MV sources. The results obtained in both papers were comparable and in our calculations we considered their findings as a conservative estimate of type B uncertainties. Specifically we assumed a linear dependence with the energy of the source following the prescription of Wulff *et al.* [20] for the NE2571 ionization chamber. Uncertainties of the various quantities calculated and of the fitting parameters are given as numbers between parentheses that affect the last significant figure, e. g., 0.16(2) means 0.16 ± 0.02 with a coverage factor $k = 1$.

As the two chambers analyzed here may be considered as an evolution of the NE2571 and NE2581 models, we compared the results obtained in the present investigation to those found for those chambers in previous works. Thus, for all $x \equiv \mathrm{TPR}^{20}_{10}(\mathrm{Q})$ values, we calculated the ratio

$$R_7(x) \;=\; \frac{k^{(\mathrm{NE2571A})}_{\mathrm{Q,Q_0}}}{k^{(\mathrm{NE2571})}_{\mathrm{Q,Q_0}}}\,, \tag{4.7}$$

that permits us to compare the results we have obtained for the NE2571A chamber with those quoted in [7] for the NE2571 one that were calculated in identical simulation conditions and showed a good agreement with those found by Muir and Rogers [6] and Wulff *et al.* [21] (calculated with the EGSnrc) and with the available experimental data [22].

It is worth pointing out here the main differences between the geometry of the NE2571A chamber analyzed in the present work and that of the NE2571 chamber studied in [7]. Table 4.1 summarizes these differences. The NE2571 geometry used in [7] was approximately reconstructed from the details found in the works by Aird and Farmer [23] and Wulff et al. [21]. The active volume is slightly smaller in the NE2571A chamber (0.69 cm^3) than in the NE2571 one (0.72 cm^3). In addition, the simulated NE2571 chamber included a PMMA sleeve with a width of 0.1 cm.

Also, our results for the NE2571A and NE2581A chambers were compared to those found for the NE2571 and NE2581 by Muir and Rogers [6] who fitted their $k_{\mathrm{Q,Q_0}}$ values by using polynomials of third degree,

$$P_3(x) \;=\; a' \;+\; b'\,x \;+\; c'\,x^2 \;+\; d'\,x^3\,. \tag{4.8}$$

Tabla 4.1: Dimensions of the various geometry elements of the NE2571A chamber considered in the present work and the NE2571 chamber studied in reference [7].

	NE2571A (this work)	NE2571 (Ref. [7])
External diameter	0.86 cm	0.82 cm
Air cavity diameter	0.63 cm	0.64 cm
Air cavity length	2.41 cm	2.40 cm
Thimble diameter	0.70 cm	0.71 cm
Thimble thickness	0.036 cm	0.040 cm
Sleeve thickness	–	0.10 cm

Specifically, the comparison was done by means of the ratios

$$R'_n(x) \;=\; \frac{k^{(\mathrm{NE25n1A})}_{\mathrm{Q},\mathrm{Q}_0}}{P_3^{(\mathrm{NE25n1})}(x)}\,, \tag{4.9}$$

for the various values of $x \equiv \mathrm{TPR}^{20}_{10}(\mathrm{Q})$.

In addition, the different fitting functions were compared directly with the ratios

$$r_7(x) \;=\; \frac{f^{(\mathrm{NE2571A})}(x)}{f^{(\mathrm{NE2571})}(x)}\,,\;\; r'_n(x) \;=\; \frac{f^{(\mathrm{NE25n1A})}(x)}{P_3^{(\mathrm{NE25n1})}(x)}\,. \tag{4.10}$$

Finally, the overall perturbation factor p_{Q} was evaluated using equation (4.1) with the stopping power ratios $(s_{\mathrm{w,air}})_{\mathrm{Q}}$ taken from [2]. Uncertainties of $(s_{\mathrm{w,air}})_{\mathrm{Q}}$ quoted in TRS-398 were considered in the evaluation of those of the p_{Q} factors. The values obtained were fitted with a linear function:

$$P_1(x) \;=\; a \,+\, b\,x\,. \tag{4.11}$$

4.3. Results and discussion

The values obtained for TPR^{20}_{10} are shown in table 4.2 where they are compared to those quoted in [7], that where calculated using an empirical expression based on ratios of percentage depth doses [2,24]. As can be seen, both calculations agree within 0.7 %.

The reference values $f_{\mathrm{c},\mathrm{Q}_0}$ obtained in our calculations were 1.117(1) for the NE2571A chamber and 1.138(1) for the NE2581A one.

The beam quality correction factors $k_{\mathrm{Q},\mathrm{Q}_0}$ found for the two ionization chambers studied here are also given in table 4.2 for the 9 beam qualities considered. In figure 4.2 these values are shown together with the corresponding fits of the function defined in equation (4.5). The values found for the fitting parameters are also given.

Tabla 4.2: Quality indexes TPR^{20}_{10} obtained by direct simulation, for the various beams considered, compared to those quoted in [7]. The uncertainty of these values is ±0.005 (with a coverage factor $k = 1$). Also shown the beam quality correction factors k_{Q,Q_0} for the NE2571A and NE2581A ionization chambers. The number in parentheses represents the statistical uncertainties, e.g. 0.983(3) means 0.983 ± 0.003 ($k = 1$).

	energy	TPR^{20}_{10}			k_{Q,Q_0}	
source	[MV]	Ref. [7]	this work	Ê	NE2571A	NE2581A
^{60}Co	–	0.571	0.573		–	–
Clinac LE	4	0.644	0.640		0.997(2)	0.994(2)
Clinac HE	6	0.670	0.673		0.985(3)	0.983(3)
	10	0.739	0.743		0.979(3)	0.972(3)
	15	0.763	0.761		0.969(3)	0.965(3)
	18	0.787	0.783		0.962(4)	0.957(4)
Siemens KD	6	0.679	0.684		0.987(3)	0.984(3)
	18	0.772	0.770		0.969(4)	0.962(4)
Elekta SL25	6	0.688	0.688		0.986(3)	0.985(3)
	25	0.799	0.800		0.959(4)	0.952(4)

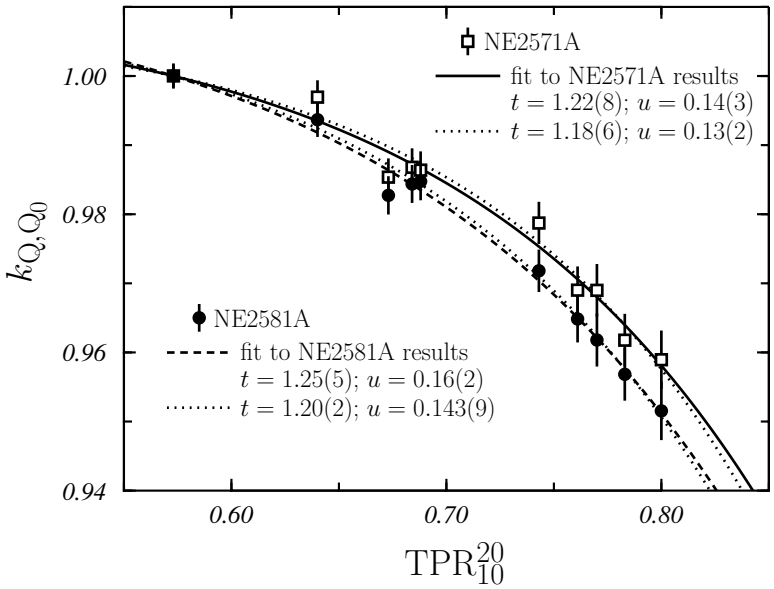

Figura 4.2: Beam quality correction factor, k_{Q,Q_0} for the NE2571A (open squares) and NE2581A (solid circles) ionization chambers, as a function of the beam quality index TPR^{20}_{10}. Uncertainties, including both systematic and statistics ones (see text), are given with a coverage factor $k = 1$. The solid and dashed curves are the fits to the results we have obtained for the NE2571A and NE2581A, respectively, using the fitting function defined in equation (4.5). The dotted curves show the fits performed neglecting the outlier point corresponding to the Clinac HE at 6 MV ($TPR^{20}_{10} = 0.673$).The values of the fitting parameters t and u are also given. The number in parentheses represents the uncertainty.

As one can see, the beam quality correction factors obtained for the NE2571A ionization chamber are slightly larger than those of the NE2581A, in all cases. The largest difference occurs at the maximum TPR_{10}^{20} where the $k_{\mathrm{Q,Q_0}}$ of both chambers differ in 0.8 %. It is worth noting the smallness of this difference even if there are significant differences between the geometries of the two chambers (different material in the thimbles and the electrodes, different diameter of the electrodes and different air active volumes).

In the results here obtained we did not find the out-of-trend behavior of the beam corresponding to the Siemens KD at 6 MV ($\mathrm{TPR}_{10}^{20} = 0.679$) that was pointed out in reference [7] for the NE2571, A12S and A19 chambers. However we have found an outlier point corresponding to the Clinac HE at 6 MV ($\mathrm{TPR}_{10}^{20} = 0.673$) which appears to be out of the fitting curve if a coverage factor $k = 1$ is considered for uncertainties. In order to investigate the role of this point in the results obtained for the fitting functions, we have performed the fits neglecting the outlier and the results are shown with dotted curves. For the two ionization chambers and in the range of the TPR_{10}^{20} values considered, the fits obtained after neglecting the outlier differ from the original ones by 0.09 % at most.

Figure 4.3 shows the different ratios that permit us to compare our results with those of the NE2571 and NE2581 chambers. In the case of the NE2571A (upper panel), we see that with the sole exception of the value corresponding to the Clinac HE at 6 MV ($\mathrm{TPR}_{10}^{20} = 0.673$), the $k_{\mathrm{Q,Q_0}}$ we have obtained for the NE2571A chamber agree within the uncertainty (with a coverage factor $k = 1$) with those of the NE2571 found in [7]

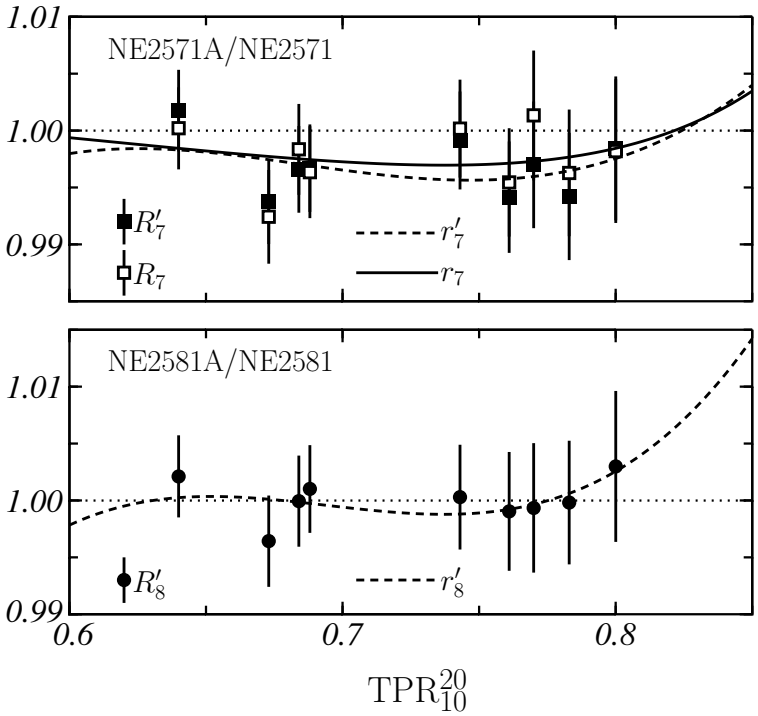

Figura 4.3: Ratios R_7 (open squares), R'_7 (solid squares), r_7 (solid curve) and r'_7 (dashed curve) for the comparison of the NE2571A/NE2571 chambers (upper panel) and R'_8 (solid circles) and r'_8 (dashed curve) for that of the NE2581A/NE2581 models (lower panel). Uncertainties, including both systematic and statistics ones (see text), are shown with a coverage factor $k = 1$.

and with those obtained from the corresponding fitting polynomial quoted in [6]. On the other hand the differences between either the ratios R_7 and R'_7 or r_7 and r'_7 (these latter found directly from the corresponding fitting functions obtained by including all data) are very small, what points out the aforementioned agreement between the calculations of references [6] and [7] for the NE2571 chamber. In this respect, it is worth mentioning that for the NE2571 chamber we obtained $f_{c,Q_0} = 1.110(2)$ [7], which is 0.6 % smaller than the value found here for the NE2571A. As the corresponding calculations were carry out in the same simulation conditions, the reason for this small difference can be ascribed to the main differences in the geometrical characteristics of both chambers that, as mentioned above, are the active volume (0.69 for the NE2571A and 0.72 for the NE2571) and the presence of a PMMA sleeve in the simulations performed for the NE2571 in [7].

In the case of the NE2581A model, the comparison is done with the results of Muir and Rogers [6]. As it can be seen in the lower panel of figure 4.3, the k_{Q,Q_0} values found for the NE2581A chamber are not significantly different from those of the NE2581 chamber. Even for the Clinac HE at 6 MV both results agree within the uncertainty (with $k = 1$).

Finally, we show in figure 4.4 the overall perturbation factors p_Q found in our calculations. Open squares correspond to the NE2571A chamber and solids circles to the NE2581A one. Solid and dashed lines show the linear fits of these results. There is a significant difference of roughly 2 % between both chambers for the reference quality, though this difference tends to reduce slightly as TPR_{10}^{20} increases. The growing slope in the

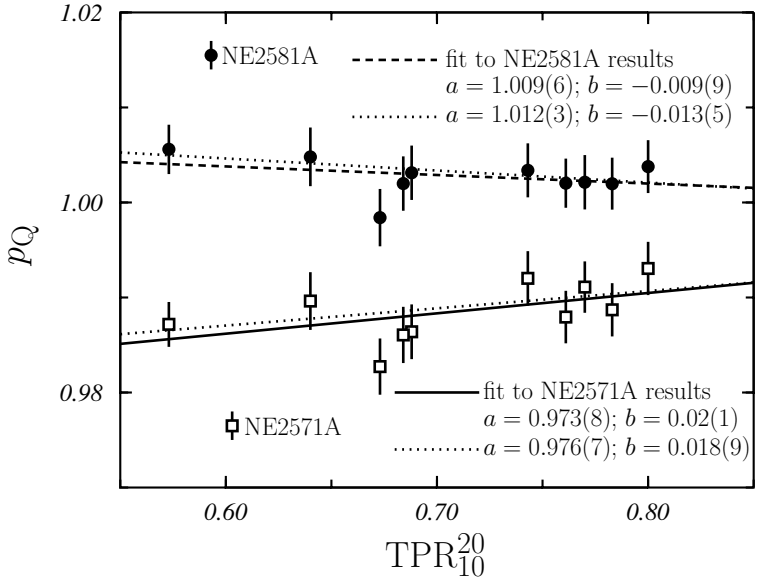

Figura 4.4: Perturbation factor, p_Q, for the NE2571A (open squares) and NE2581A (solid circles) ionization chambers, as a function of beam quality index TPR_{10}^{20}. Uncertainties are given with a coverage factor $k = 1$. The lines are linear fits, as given by equation (4.11), to the results obtained for the two chambers. The values of the fitting parameters are also given. The dotted curves show the fits performed neglecting the outlier point corresponding to the Clinac HE at 6 MV ($TPR_{10}^{20} = 0.673$). Here, the number in parentheses represents the statistical uncertainty, e.g. 0.972(9) means 0.971 ± 0.009.

NE2571A chamber ($b = 0.02(1)$) is close to the value we found for the NE2571 chamber in [7] ($b = 0.030(7)$). On the other hand, the values found for the NE2581A chamber show up rather independent of the beam quality. Again we found the out-of-tendency behavior of the value corresponding to the Clinac HE at 6 MV that also appeared for k_{Q,Q_0} (see figure 4.3). As in that case, we have done the fits of the p_Q values neglecting this outlier point and the results have been plotted with dotted lines. The maximum difference between the two fits for each chamber is 0.09 % and occurs for the ^{60}Co Q_0 beam quality ($TPR_{10}^{20} = 0.573$).

4.4. Conclusions

In this work, the beam quality correction factor has been calculated for the NE2571A and NE2581A ionization chambers with the Monte Carlo code PENELOPE for a TPR_{10}^{20} range from 0.64 to 0.80, that corresponds to linac photon beams between 4 and 25 MV.

The values of k_{Q,Q_0} obtained for the NE2571A chamber are, at most, 0.8 % larger than those found for the NE2581A. In general, the results we have found for the NE2571A and NE2581A chambers agree within uncertainties with those quoted in previous works for their predecessors NE2571 and NE2581 chambers, respectively.

Acknowledgements

This work has been supported in part by the Junta de Andalucía (FQM0220), the Spanish Ministerio de Economía y Competitividad (FPA2012-31993) and the European Regional Development Fund (ERDF).

[1] Almond PR, Biggs PJ, Caursey BM, Hanson WF, Saiful HM, Nat R, Rogers DWO. AAPM's TG-51 protocol for clinical reference dosimetry of high-energy photon and electron beams. Med Phys 1999; 26: 1847-70.

[2] International Atomic Energy Agency. Absorbed dose determination in external beam radiotherapy, IAEA Technical Reports Series 398. Vienna: IAEA; 2000.

[3] Andreo P. Absorbed dose beam quality factors for the dosimetry of high-energy photon beams. Phys Med Biol 1992; 37: 2189-211.

[4] Sempau J, Andreo P, Aldana J, Mazurier J, Salvat F. Electron beam quality correction factors for plane-parallel ionization chambers in high energy photon beams: Monte Carlo calculations using the PENELOPE system. Phys Med Biol 2004; 49: 4427-44.

[5] Capote R, Sánchez-Doblado F, Leal A, Lagares JI, Arráns R, Hartmann GH. An EGSnrc Monte Carlo study of the microionization chamber for reference dosimetry of narrow irregular IMRT beamlets. Med. Phys. 2004; 31: 2416-22.

[6] Muir BR, Rogers DWO. Monte Carlo calculations of k_Q, the beam quality conversion factor. Med Phys 2010; 37: 5939-50.

[7] F Erazo, AM Lallena. Calculation of beam quality correction factors for various thimble ionization chambers using the Monte Carlo code PENELOPE. Physica Medica: Eur. J. Med. Phys. 2013; 29: 163-70.

[8] Salvat F, Fernández-Varea JM, Sempau J. PENELOPE: a code system for Monte Carlo simulation of electron and photon transport. Paris: Nuclear Energy Agency; 2011.

[9] Chica U, Anguiano M, Lallena AM. Benchmark of PENELOPE for low and medium energy x-rays. Physica Medica: Eur. J. Med. Phys. 2009; 25: 51-7.

[10] Chica U, Flórez G, Anguiano M, Lallena AM. A simple analytical expression to calculate the backscatter factor for low energy X-ray beams. Physica Medica: Eur. J. Med. Phys. 2011; 27: 75-80.

[11] Miras H, Terrón JA, Lallena AM. Monte Carlo simulation of COMS ophthalmic applicators loaded with Bebig I25.S16 seeds and comparison with planning system predictions. Physica Medica: Eur. J. Med. Phys. 2013; 29: 670-6.

[12] Juan-Senabre XJ, Porras I, Lallena AM. A simple modification of TG-43 based brachytherapy dosimetry with improved fitting functions: Application to the selectSeed source. Physica Medica: Eur. J. Med. Phys. 2013; 29: 403-11.

[13] Guerrero R, Almansa JF, Torres J, Lallena AM. Dosimetric characterization of the ^{60}Co BEBIG Co0.A86 high dose rate brachytherapy source using PENELOPE. Physica Medica: Eur. J. Med. Phys. 2014; 30: 960-67.

[14] Erazo F, Brualla L, Lallena AM. Electron beam quality $k_{\mathrm{Q,Q_0}}$ factors for various ionization chambers: A Monte Carlo investigation with PENELOPE. Phys. Med. Biol. 2014; 59: 6673-91.

[15] Sempau J, Badal A, Brualla L. A PENELOPE-based system for the automated Monte Carlo simulation of clinacs and voxelized geometries-application to far-from-axis fields. Med. Phys. 2011; 38: 5887-95.

[16] Badal A, Sempau J. clonEasy: A package of linux scripts for the parallelization of Monte Carlo simulations. Comp Phys Comm 2005; 175: 440-50.

[17] Mora GM, Maio A. Monte Carlo simulation of a typical ^{60}Co therapy source. Med Phys 1999; 26: 1847-70.

[18] Sheikh-Bagheri D, Rogers DWO. Monte Carlo calculation of nine megavoltage photon beam spectra using BEAM code. Med Phys 2002; 29: 391-402.

[19] Kawrakow I. On the effective point of measurement in megavoltage photon beams. Med Phys 2006; 33: 1829-39

[20] Wulff J, Heverhagen JT, Zink K, Kawrakow I. Investigation of systematic uncertainties in Monte Carlo-calculated beam quality correction factors. Phys Med Biol 2010; 55: 4481-93.

[21] Wulff J, Heverhagen JT, Zink K. Monte Carlo based perturbation and beam quality corrections factors for thimble ionization chambers in high energy photon beams. Phys Med Biol 2008; 53: 2823-36.

[22] Nederlandse Commissie voor Stralingsdosimetrie. Code of practice for the absorbed dose determination in high energy photon and electron beams. NCS Report 18. Delft: NCS; 2008.

[23] Aird EG, Farmer FT. The design of a thimble chamber for the Farmer dosemeter. Phys Med Biol 1972;17:169-74.

[24] Followill DS, Tailor RC, Tello VM, Hanson WF. An empirical relationship for determining photon beam quality in TG-21 from a ratio of percent depth doses. Med Phys 1998; 25: 1202-5.

Capítulo 5

CONCLUSIONES Y PERSPECTIVAS

En este trabajo se han evaluado mediante simulación Monte Carlo con el código PENELOPE los factores de corrección de calidad de haz, k_{Q,Q_0}, para varias cámaras de dedal y plano-paralelas y para haces de fotones y electrones.

En el caso de la cámara de ionización tipo dedal NE2571, que es considerada de referencia en la dosimetría física, los valores de k_{Q,Q_0} para haces de fotones están en excelente concordancia con los valores reportados en la bibliografía calculados usando el código EGSnrc y también con los obtenidos experimentalmente. Todos estos valores difieren de manera significativa de los factores establecidos en el protocolo TRS-398, diferencia que se incrementa con el aumento de la energía nominal de los haces. Esto sugiere que los valores del protocolo del Organismo Internacional de Energía Atómica, que son usados en la práctica clínica, deben ser revisados.

Los factores globales de perturbación p_Q para esta misma cámara NE2571 presentan diferencias significativas con los valores obtenidos con EGSnrc por otros autores. Esta diferencia es de alrededor del 0.4 % para el ^{60}Co y se mantiene casi constante (sólo con un ligero incremento) conforme aumenta el valor de la energía del haz.

Los valores de k_{Q,Q_0} para las cámaras de Standard Imaging A19 y A12S, usadas en la dosimetría de radioterapia convencional y estereotáxica, respectivamente, están de acuerdo con los valores reportados en la bibliografía obtenidos con EGSnrc o determinados experimentalmente. Los factores k_{Q,Q_0} para estas dos cámaras de ionización no están reportados en el TRS-398. Los valores de los factores de perturbación p_Q para estas dos cámaras de ionización se diferencian de los obtenidos con EGSnrc de forma similar a la ya discutida para la cámara NE2571.

Se han calculado los factores de corrección k_{Q,Q_0} en el caso de haces de electrones y para siete cámaras plano-paralelas de Standard Imaging: A10, A11, A11TW, P11, P11TW, T11 y T11TW. Se han considerado varios haces de electrones realistas obtenidos para un acelerador Varian Clinac 2100 C/D y los haces monoenergéticos sintonizados para reproducir los valores de R_{50} de los mismos. Para todas las cámaras de ionización analizadas se han calculado los factores de corrección para dos tamaños de campo de referencia: $10 \times 10\,\mathrm{cm}^2$ y $20 \times 20\,\mathrm{cm}^2$. Los valores obtenidos para el primero son ligeramente más altos que los del campo de $20 \times 20\,\mathrm{cm}^2$; la mayor diferencia (alrededor del 0.8 %) se ha encontrado para la cámara de ionización A10 (la de menor volumen activo de recolección de carga) y para electrones con una energía nominal de 9 MeV. En cualquier caso, los resultados encontrados para los dos tamaños de campo son estadísticamente compatibles en todos los casos para un factor de cobertura de $k = 2$.

Para energías nominales inferiores a 12 MeV, los valores de k_{Q,Q_0} obtenidos para los haces provenientes de la simulación detallada de los aceleradores lineales y los de los haces monoenergéticos sintonizados están en buen acuerdo. Sin embargo, para energías mayores, los factores correspondientes a los haces realistas son alrededor del 1 % superiores a los de los monoenergéticos. Este resultado contradice el de un trabajo previo en el que no se encontraron diferencias entre ambos tipos de cálculos en el caso de las cámaras PPC-05 y PPC-40, de Wellhöfer, y NACP02. Específicamente se han realizado los cálculos para esta última cámara encontrando las mismas diferencias que para las otras cámaras, diferencias que han podido ser asignadas, al menos en una parte importante, a los fotones secundarios producidos en los distintos elementos del acelerador así como en el aire existente ente el cabezal del mismo y el maniquí de agua donde se acumula la dosis.

Para las cámaras Standard Imaging se ha puesto de manifiesto la importancia de los materiales de construcción que pueden dar lugar a factores de corrección que muestran diferencias significativas.

Por último se han evaluado los factores de corrección k_{Q,Q_0} para las cámara NE2571A y NE2581A para los haces de fotones ya considerados en el caso de las otras cámaras de dedal analizadas. Los valores obtenidos para la primera son ligeramente superiores a los de la segunda, si bien están respectivamente de acuerdo con los factores encontrados para sus cámaras predecesoras (NE2571 y NE2581) en trabajos previos.

El trabajo desarrollado en esta tesis ha permitido establecer una metodología de cálculo de factores de corrección de calidad de haz que permite evaluar dichos factores de manera fiable, tanto para haces de fotones como de electrones y para cámaras de ionización cilíndricas y plano-paralelas. Las diferencias que hemos encontrado entre los resultados obtenidos con PENELOPE y con EGSnrc pone de manifiesto la necesidad de completar los cálculos para otras cámaras a fin de establecer de forma unívoca los valores de los factores que deben ser utilizados en la práctica clínica.

Por otro lado, una de las cuestiones pendientes para facilitar los cálculos es la de incorporar en los mismos técnicas de reducción de varianza. Este aspecto es fundamental para poder abordar los cálculos sobre todos en el caso de cámaras de volumen pequeño para las que las simulaciones requieren un tiempo de CPU más que considerable.

INFORME

Esta tesis doctoral se basa en los artículos que a continuación se relacionan y sobre los cuáles se proporcionan los indicios de calidad correspondientes.

1. F. Erazo and A.M. Lallena
   Calculation of beam quality correction factors for various thimble ionization chambers using the Monte Carlo code PENELOPE
   Physica Medica: European Journal of Medical Physics 29 (2013) 163-170
   Factor de impacto: 2.403
   Posición: 44 de 125
   Categoría: RADIOLOGY, NUCLEAR MEDICINE & MEDICAL IMAGING

2. F. Erazo, L. Brualla and A.M. Lallena
   Electron beam quality k_{Q,Q_0} factors for various ionization chambers: A Monte Carlo investigation with PENELOPE
   Physics in Medicine and Biology 59 (2014) 6673-6691
   Factor de impacto: 2.761
   Posición: 34 de 125
   Categoría: RADIOLOGY, NUCLEAR MEDICINE & MEDICAL IMAGING
   Posición: 21 de 76
   Categoría: ENGINEERING, BIOMEDICAL

3. F. Erazo and A.M. Lallena
   Photon beam quality correction factors for the NE2571A and NE2581A thimble ionization chambers using PENELOPE
   Physica Medica: European Journal of Medical Physics (2015) [en prensa]
   Factor de impacto: 2.403
   Posición: 44 de 125
   Categoría: RADIOLOGY, NUCLEAR MEDICINE & MEDICAL IMAGING

Algunos de los resultados de esta tesis doctoral se han presentado en el congreso que a continuación se indica

1. F. Erazo, L. Brualla and A.M. Lallena
   Electron beam quality correction factor for ionization chambers: monoenergetic electrons versus linac phase-spaces
   20 Jahrestagung der Deutschen Gesellschaft für Radioonkologie. Düsseldorf (Alemania) 2014
   Strahlentherapie und Onkologie 190 Suppl. 1 (2014) 145.